

The Dynamics of the cD Clusters Abell 119 and Abell 133

M.J. Way¹, H. Quintana^{2,3} and L. Infante

Department of Astronomy and Astrophysics, P. Universidad Catolica de Chile,
Casilla 104, Santiago 22 , Chile

I: mway@newton.umsl.edu

Received _____; accepted _____

arXiv:astro-ph/9709036v1 4 Sep 1997

¹present address: Department of Physics and Astronomy, University of Missouri-St.Louis,
8001 Natural Bridge Rd., St.Louis, MO 63121-4499

²Visiting Astronomer, Las Campanas Observatory of The Carnegie Institute of
Washington

³1995 Presidential Chair in Science

ABSTRACT

A dynamical analysis of the structure of the clusters of galaxies Abell 119 and Abell 133 is presented, using new redshift data combined with existing data from the literature. We compare our results with those from the X-ray data for these clusters, and with those from radio data for the central cD galaxy in each cluster. A comparison of the mass estimate based on X-ray data and that obtained here after subgroups are eliminated shows them to be comparable. After the elimination of subgroups, 125 galaxy members in Abell 119 and 120 in Abell 133 give dispersions of 472 km s^{-1} and 735 km s^{-1} respectively. However, our dynamical analysis of the optical data shows little substructure in the velocity field of Abell 133, conflicting with what is seen in the Rosat X-ray map. Abell 119 seems to have multiple structures along the line of sight. We derive virial mass estimates of $3.05 \times 10^{14} M_{\odot}$ for Abell 119 and $7.79 \times 10^{14} M_{\odot}$ for Abell 133 within $1.5 h^{-1} \text{ Mpc}$, which agree well with the X-ray-derived masses within errors.

Subject headings: clusters: galaxies

1. Introduction

Regular, rich clusters of galaxies are the largest objects in the Universe likely to be bound and possibly relaxed. Their differing shapes, concentrations and populations are customarily interpreted as representing different stages in the gravitational evolution of the matter of the cluster. The most regular clusters usually have galaxies of type cD at their centers. The view that such clusters have reached stationary equilibrium is generally accepted. However, recent work has shown the presence of significant substructure in these clusters, challenging the virialization and relaxation hypothesis. To search for substructure one need not only look at the distribution of galaxies, but to analyze the gas profiles and inhomogeneities as revealed by the X-ray data and the dynamical information provided by the velocity field of the galaxies throughout the cluster.

The nearby cD clusters Abell 119 and Abell 133 are among the brightest sources in X-rays. As such, they were promising sources to be studied in depth in the optical and X-ray bands. Together with other clusters accessible to our southern programs, they were chosen to carry out a deeper velocity survey using multi-fiber spectrographs. Here we report velocities taken with the Las Campanas DuPont 100" telescope.

In Section II we discuss how the data were obtained. We then explain the data reduction in section III, and in IV we detail how velocity data from the literature compares with this paper's data, and how it was integrated to our data for analysis. The dynamical analysis is presented in section V, broken up into several subsections for Abell 119 and 133. Finally, section VI contains a discussion and the implications of our analysis.

2. Observations

The aim of our program was to obtain velocities for as many galaxies as possible over a reasonably wide field, within the observational allocation of time. We chose to survey areas of $1.5^\circ \times 1.5^\circ$ centered on the cD galaxies, the field covered by 100" DuPont telescope fiber spectrograph. Lacking previous photometric data to select a magnitude limited sample, we measured the positions of galaxies clearly identified on the glass copies of the Palomar Sky Survey at ESO, Garching. The plates were searched by eye on the Optronics machine monitor following strips in declination. The final astrometric lists contained some 400 galaxies in each cluster and a number of stars used for guiding the fiber arrays. The positions were determined from astrometric solutions based on 25 SAO or Perth reference stars, using standard programs at ESO. Their relative accuracy is 0.3 arcsec rms. However, the external accuracy should be of order 2 arcsec. See figures 1a and 1b for plots of the x-y positions. Notice in figure 1b that the bottom of the plot is blank because the entire field of Abell 133 is close to the edge of the scanned Palomar plate. We could not use a second plate to obtain the rest of the velocities because the external positional error between plates was too high.

We used Shectman's fiber spectrograph (Shectman 1985) mounted on the 100" telescope on the nights of 22-25 October 1990. The multi-fiber system consists of a plug plate at the focal plane to which 65 fibers are attached and run to a Boller and Chivens spectrograph coupled to a 2DFrutti detector (2DF). A 600 line mm^{-1} grating blazed at 5000\AA was set at an angle $9^\circ 40'$, giving a wavelength coverage from $\sim 3800\text{-}6800\text{\AA}$. Normally, 50-55 fibers are used for objects. Ten sky fibers are set aside, spaced at intervals of one every 6 fibers along the spectrograph entrance, and positioned in a random pattern in the plug plate. The resulting 2DF image has a 1520×1024 pixel area, with a dispersion of $\sim 2.6\text{\AA} \text{ pixel}^{-1}$ and a final resolution of $\sim 10\text{\AA}$. The fiber images are ~ 8 pixels wide, and

separated by ~ 12 pixels from center to center.

Exposure times were adjusted to be between 80 and 120 minutes, depending on the brightness of the selected galaxies for each exposure. The 2DF detector is a photon counting system where one can view the current exposure at any stage. In this way one can obtain the optimum exposure time for a field. A faintness limit of ~ 17.5 magnitudes in R was reached. 150 spectra in each of Abell 133 and Abell 119 were obtained in this run. Quartz lamp exposures were used to correct for pixel to pixel variations of the detector. To properly illuminate the whole detector surface the grating angle was changed to several values on these exposures. As well, helium-neon comparison lamp exposures were taken off the wind-screen for wavelength calibration before and after each exposure. The 2DFrutti detector has a small dark current and no corrections were made for that effect.

3. Reductions

Velocity determinations were carried out using a cross-correlation technique *and* by identifying and fitting by eye line profiles. All reductions were performed inside of the IRAF(Tody 1993) environment. For a complete discussion of the reductions see Quintana et al. 1996(hereafter QRW96). That described below is a summary of the reductions. Due to the nature of the fiber+2DFrutti system typical S shaped distortions are inherent in this instrument. A sixth order spline3 curve was used to trace the S shaped spectra. The IRAF HYDRA package was used to extract the spectra, correct pixel to pixel variations via the dome flat, use a Fiber Transmission Table for appropriate sky subtraction and put the spectra on a linear in wavelength scale. The wavelength solutions for 20-30 points using a 5, 6, or 7 order Chebyshev typically yielded residual values less than 0.4 rms \AA , where 1 pix $\sim 2.6\text{\AA}$. The ten sky spectra from each exposure were combined via a median filter and subtracted from each of the object spectra.

Two different methods were used to measure the redshift of the objects. For normal early type spectra the RVSAO (Kurtz et al. 1991) cross-correlation algorithm supported inside IRAF was used. The algorithm used in RVSAO is described in Tonry & Davis 1979 (hereafter TD79). A reliability factor was generated by RVSAO called the R value (see TD79 for details). Normally a low R value ($R \leq 4$) indicated a need to look at the spectra and try line by line Gaussian fitting (the second method). To utilize RVSAO *template* spectra with high signal to noise and well determined radial velocities were needed. Two of the four templates used in this paper were galaxy spectra taken with the fiber instrument, NGC 1407 and NGC 1426, another galaxy (NGC1700) was from the previous detector on the 2.5 meter at Las Campanas (Spectrograph), and one was a synthetic template. The synthetic template was constructed from the excellent library of stellar spectra of Jacoby et al. 1984. We used ratios of stellar light for the E0 galaxy NGC1374 from the synthesis studies of Pickles 1985. In the end it was found that the template which gave the lowest error value out of the four radial velocity cross-correlation templates mentioned above proved to have more consistent results. For non-early type spectra (i.e emission lines, E+A, etc.) a line by line Gaussian fit was used and the resulting velocities from each line fit were averaged.

Tables 1 (Abell 119) and 2 (Abell 133) give the velocity results, where column 1 shows the identification number, columns 2 and 3 give 1950.0 epoch positions, and columns 4, 5, 6, 7 and 8 give the individual velocity values, their errors (1σ), the corresponding TD79 R values or number of measured lines (mostly emission) if the R number was too low for a proper velocity determination, references, and the identification number from each reference. Columns 9 and 10 give the final adopted velocities, if averaged, and their respective one σ errors.

Multiple measurements and integrated velocity values from the literature were

combined and are described in the next section. Where large discrepancies exist with values quoted in the literature, they have been eliminated as indicated in the comments. The individual velocities retained have been averaged and weighted by the corresponding quoted errors (combined in quadrature) for an estimate of the final error.

For a number of galaxies 2 spectra were measured. This allows a check on internal consistency. These velocities are listed for the corresponding galaxies in Tables 1 and 2. In Abell 133 there are six galaxies with two measurements which differ by values from 6 to 75 km s⁻¹, just within the errors, showing good internal consistency. In Abell 119 five galaxies have 2 fiber spectra with differences ranging from 7 to 117 km s⁻¹. The only galaxy not falling within the quadratically added errors was number 25370 where the difference was 117 km s⁻¹ which can be attributed to the low signal to noise in one of the spectra obtained.

4. Comparison

A zero point shift for references with several velocities in common can be used to bring the data to a common system. This has been applied before averaging weighted by the respective errors (see QRW96 for details). The first systematic determination of velocities in Abell 119 was done by Melnick & Quintana 1981 (hereafter MQ81), who published 23 velocities, with typical errors 100-250 km s⁻¹. For 19 galaxies a systematic shift was found between this paper (fibr) and MQ81 (figure 2a) of $\sim -45 \pm 217$ km s⁻¹ rms after applying a σ clipping routine that rids one of those MQ81 velocities quoted with errors larger than 150 km s⁻¹ (with the exception of one). As noted in MQ81, errors larger than 150 km s⁻¹ denote very uncertain velocities, a fact borne out by the new measurements. It is also noted that the position of galaxy 10 in MQ81 is wrong (due to a re-numbering of galaxies in that paper). Fabricant et al. 1993 (hereafter FAB93) give values for 60 velocities. Of the FAB93 velocities 48 are in common with this paper's fiber data. In comparison with

FAB93 (see figure 2b) there is a systematic shift of $\sim -28 \text{ km s}^{-1}$ with an RMS of $\sim 76 \text{ km s}^{-1}$. For completeness, in Table 1 12 galaxies are included with velocities measured solely by FAB93. Several velocity measurements in Abell 119 are added from the papers of Zabludoff et al. 1993 (2 measurements), de Vaucouleurs et al. 1991 (4), Huchra et al. 1983 (1), Sandage 1978 (1), and Kinman & Hintzen 1981 (1). A comparison with the two velocities in common with Zabludoff et al. 1993 show a systematic shift of $5 \sim -45 \pm 86 \text{ km s}^{-1}$ rms. In Abell 133 overlapping velocities were found in the papers of Merrifield & Kent 1989 (3), and de Vaucouleurs et al. 1991 (5). In Merrifield & Kent 1989 a shift of $-134 \text{ km s}^{-1} \pm 64$ rms was found. Using the 9 velocities in common with Abell 133 and Abell 119 from de Vaucouleurs et al. 1991 a systematic shift of $-34 \text{ km s}^{-1} \pm 81$ rms was found. All of the shifts above suggest that it is this paper’s data which is shifted by roughly 40 km s^{-1} with respect to the literature.

5. Dynamical Analysis

5.1. Abell 119

5.1.1. 1D tests (velocity space)

Information from the 1D velocity distribution was obtained with ROSTAT, a program for robust estimation of velocity distributions based on the work of Beers et al. 1990 and kindly distributed by Tim Beers. ROSTAT was first used to calculate the robust estimators of location C_{BI} (average) and scale S_{BI} (dispersion) with 10000 bootstraps and with 90% confidence intervals (see Table 3). As a first order attempt to remove outlier galaxies in the velocity distribution a standard 3σ (S_{BI}) clipping of Yahil & Vidal 1977 was used. Consequently, all galaxies in Abell 119 closer than 11033 and further than $15609 \text{ km sec}^{-1}$ were eliminated. This 3σ clipped data is taken as defining *the cluster*. Then *the cluster* data

is taken through a second ROSTAT run using those points within the velocity ranges above to utilize the shape estimators of skewness, kurtosis, tail and asymmetry. Their values are listed in Table 3. For a thorough discussion of these estimators see Bird & Beers 1993.

Of the 4 estimators only the robust estimator of asymmetry shows no strong deviation from a Gaussian distribution, but note that the robust estimators, asymmetry and tail, are normally much more conservative and will give fewer false positives for non-Gaussian distributions than the classical skewness and kurtosis. The high positive kurtosis (leptokurtic) value leads one to believe the tails are heavier than expected for a Gaussian. The large positive value of skewness implies a lack of values below C_{BI} or that values on the positive side of C_{BI} are more enhanced than a standard Gaussian distribution. The tail index points to a double exponential shape rather than Gaussian. Given these indicators of non-Gaussian behavior the KMM objective partitioning algorithm was used to search for multiple Gaussians in the velocity field. See Ashman et al. 1994 for a detailed discussion. Briefly, KMM fits a user-specified number of Gaussians to the velocity data and estimates the improvement of the multiple Gaussian fit versus a single Gaussian. The user first inputs an estimate of the positions of the multiple Gaussians. Using the velocity histogram (figure 3a) as a starting point two, three, four, and five Gaussians were fit to the data. For the three Gaussian fit, Gaussians were first estimated at 11900, 13200, and 14650 km sec⁻¹ from the velocity histogram. The program returned values of 11837, 13253 and 14718 km sec⁻¹ with a rejection of the single Gaussian model at a confidence level of 97.9%. This three Gaussian model implies that two smaller groups are projected or in-falling toward the main cluster body, one from the front and one from the back. In fact FAB93 detected the foreground group as having velocities less than 12000 km sec⁻¹, but miss the background group. In figure 4 the three groups are over plotted. *Group 1* is denoted by \square (11 members), *group 2* by \bullet (125 members) and *group 3* by $+$ (17 members). Further attempts to subdivide *group 2* using KMM were unsuccessful. Running ROSTAT on the 3 groups provides one

with further information. *Group 1* has a large negative skewness implying a distribution with depleted values above the mean velocity. *Group 3* is the reverse with positive skewness implying depleted values below the mean velocity. The kurtosis values for both are a little high implying heavy tails. The tail index for *group 1* has a CN(0.20,3) distribution shape according to Table 1 of Bird & Beers 1993, where 20% of the points within a Gaussian width of 3σ are bad. In *group 3* the kurtosis value of 1.222 points to a double exponential distribution. This would lead one to believe that the groups are being pulled apart by the gravitational field of *group 2*, distorting their distributions.

A histogram of velocities for *group 2* is presented in figure 3b. All galaxies were within 3σ of each other and the results for C_{BI} , S_{BI} , skewness, kurtosis, asymmetry, and tail are shown in Table 3. The skewness and asymmetry indices imply a Gaussian distribution. The kurtosis index once again points to a tailed Gaussian distribution and the tail index implies that we have a normal distribution. Further analysis on *group 2* using 2D and 3D estimators demonstrate that these are probably false positive rejections of a Gaussian distribution, see following subsections.

5.1.2. *cD velocity offset, Z_{score}*

In relaxed clusters the cD galaxy should sit at the bottom of the potential well, thus they should be at the center of the velocity distribution (Quintana & Lawrie 1982), which is borne by $\sim 70\%$ of cD clusters (Bird 1994). A significant cD galaxy velocity offset from the cluster mean (or the Z_{score} , Gebhardt & Beers 1991) may be an indicator of substructure. Bird 1994 has shown that if one attempts to identify the cD galaxy’s host clump, using the methods in this paper to eliminate non-cluster members, that most cases of “speeding cDs” disappear.

In Table 4 the Z_{score} values for *the cluster* and *group 2* are presented. One can see that the Z_{score} for *group 2* is slightly larger than that for *the cluster*, but the Z_{score} with bootstrapped errors bracket zero which would *not* indicate a significant velocity offset, implying that the Abell 119 cD is indeed sitting at the center of it’s host clump. The host clump being *group 2*, which has a qualitatively similar Z_{score} value. It can be seen that the fore and background clumps might tend to balance out the Z_{score} of *the cluster* because it is dependent solely on the measured 1-D radial velocities of galaxies.

5.1.3. 2D and 3D tests

To further test *the cluster* and *group 2* data several 2 and 3 Dimensional substructure tests were used. The Lee statistic (Fitchett M.J. 1988) tests a 2D dataset for the presence of 2 equal sized groups versus 1. The 3D Dressler & Schectman 1988 Δ test, West & Bothun 1990 α test, and Bird 1994 ϵ test all look for clumping in the spatial *and* velocity data. The test results are presented in Table 4. The Lee statistic results for *the cluster* dataset imply a null result for the two group fit because of the low value of L_{RAT} and a p value of 117 (where p less than 25 implies a statistically significant amount of substructure). On the other hand a plot of the Lee statistic distribution (figure 5a) can help to define an elongation axis, if any, of the 2D distribution. The highest point in figure 5a defines the elongation axis of *the cluster* to be $\phi_{max}=86.4^\circ$. Any multiple peaks seen in the Lee statistic plot may be an indicator of more complex structure, even given the low L_{RAT} , but there are no multiple peaks here. The Lee statistic applied to *group 2* has a slightly higher value of L_{RAT} , but the p value still rejects any statistically significant substructure. The Lee statistic for *group 2* plotted in figure 5b differs little from that of *the cluster* in figure 5a. The elongation axis $\phi_{max}=86.4^\circ$ seen in *the cluster* plot of 5a (the peak in 5a) has vanished.

In contrast all of the 3D tests (Table 4) report null for the substructure hypothesis in

the cluster data even though two in-falling clumps along the line of sight (LOS) were found using KMM, but tests done by Bird 1993 indicate that the 3D tests are insensitive to LOS mergers!

2D and 3D tests were also applied to *group 2*. Since the foreground and background groups were along the LOS of “the cluster” and are more or less evenly distributed in RA and DEC (see figure 4) one would not expect to see much of a difference in comparison with *the cluster* data. The Lee statistic for *group 2* has a slightly higher value of L_{RAT} , but the p value still rejects any statistically significant substructure. The Lee statistic result for *group 2* is plotted in figure 5b. It does not differ greatly from that of *the cluster* dataset showing the elongation angle $\phi_{max}=82.8^\circ$.

Of the three 3D tests only the Δ test statistic gave a positive rejection of the Gaussian hypothesis. This may be a false positive since no other estimators gave the same result and, as pointed out by Bird 1993, the Δ test is the more optimistic of the three. This result coupled with a low L_{RAT} for *group 2* from the Lee statistic lends support to the 3D tests null result.

5.1.4. Rotation

As pointed out by Malumuth et al. 1992 a smooth gradient in the velocity field may complicate use of the Δ statistic by giving a false positive substructure result. Even though in Abell 119 the Δ statistic has a null hypothesis for *the cluster* data set one is still interested in knowing whether clusters in general show signs of rotation. An estimate of cluster rotation can be made by calculating a binned C_{BI} along the elongation axis (as defined by the Lee statistic). Figure 6a shows $C_{BI}(R)-C_{BI}(\text{global})$ versus R with 90% bootstrapped confidence intervals. There is no clear gradient in the data and therefore

implies little in the way of cluster rotation. There is however a strong discontinuity at radii of around $1 \text{ h}^{-1}\text{Mpc}$. This *could* just be a sampling effect. If one looks at the original positions as measured from the ESO plates (figure 1a) one cannot help but see two “voids” in the lower left hand corner and upper right hand corner at about $1 \text{ h}^{-1}\text{Mpc}$ in radius. This also manifests itself in the measured velocities (figure 4).

For *group 2* (figure 6b) much the same situation as above is found. No clear gradients seem to exist, although the discontinuous feature at $\sim 1 \text{ h}^{-1}\text{Mpc}$ persists, as expected. This result would tend to support the Δ test finding of substructure in *group 2* given a lack of evidence for any strong velocity field gradients.

5.1.5. *Velocity Dispersion Profile (VDP)*

Variations in the velocity dispersion with radius may indicate a condition of non-equilibrium (Kaiser 1987). To test this for “the cluster” figure 7a plots radius versus velocity. The caustics for “the cluster” data are well defined except for three points at the top of figure 7a. Eliminating these three points (which are actually part of the background group picked with KMM) a plot of the cumulative S_{BI} (velocity dispersion) versus radius is shown in figure 8a. As one can see in figure 8a, the velocity dispersion falls with radius as is seen with many well studied rich clusters (e.g. Abell 3266 in Quintana et al. 1996, and others in den Hartog & Katgert 1996).

For *group 2* radius versus velocity is show in figure 7b and cumulative velocity dispersion versus radius in figure 8b. Now the situation has changed dramatically. Both plots show a roughly flat distribution, even out to large radii. Either the fore and background groups have been eliminated incorrectly (which is not supported by the previous work of Fabricant et al. 1993 nor the X-ray data) or one is witnessing the effects of velocity anisotropies

in the central region (Fadda et al. 1996) where the effects of dynamical friction may be slowing down the more luminous central galaxies. One may recall that the frictional force is proportional to the local matter density (Chandrasekhar 1943) which is higher in the central region of a cluster. As well, den Hartog & Katgert 1996 agree that it may be anisotropic projection effects that cause inverted VDPs. *Group 2* does not have an inverted VDP, but it may help to explain the flat VDP seen.

5.1.6. *Rosat versus AKM*

Using the adaptive kernel map (AKM) first applied by Beers et al. 1991 to the 2-D galaxy distribution one can attempt to make a comparison between the contours generated from the number density of galaxies deemed to be in *group 2*, and that from the X-ray density contours of Rosat.

Figures 9a and 9b show the Rosat and AKM contour optical overlays for a 1.5×1.5 h^{-1} Mpc region centered on the central cD. The data is restricted to the inner $1.5 h^{-1}$ Mpc since at this redshift that is the extent to which one can gain meaningful information from the X-ray data.

The Rosat X-ray data in figure 9b has been smoothed with a 2 pixel FWHM Gaussian using the `imsmooth` task in the PROS¹ X-ray reduction package. The image was obtained from the publically released HEASARC Rosat CD Volume 2 (Corcoran et al. 1994).

Since both the AKM and Rosat data presented in figures 9a and 9b cover the same $1.5 \times 1.5 h^{-1}$ Mpc region a direct, albeit qualitative, comparison of the matter density

¹PROS is developed, distributed, and maintained by the Smithsonian Astrophysical Observatory, under partial support from NASA contract NAS5-30934

(Rosat/X-ray) to the 2-D galaxy number density can be made. It is obvious that a NNE elongation in the central regions of both plots manifests itself and in fact coincides with the elongation axis *objectively* obtained using the Lee test statistic. This strong evidence suggests that if one obtains enough galaxy redshifts in a cluster one can accurately begin to estimate the local matter density with confidence.

5.1.7. Radio

The core of Abell 119 has been radio mapped at 20cm with the VLA by Zhao et al. 1989. They claim the elongation of the cD may indicate a Wide Angle Tailed source. The NNW elongation seen in the radio mapped cD does not correspond to the large scale NNE elongation seen in this cluster. If the cluster had formed recently one might expect to find the radio structure mimicking the larger scale structure, but since this is not the case it is presented as evidence that *group 2* was not recently formed, and since one would expect more substructure with younger systems it further supports the lack of substructure seen in the velocity field.

5.1.8. Mass

In Table 5 the mass estimates of the *three groups* are reported. The virial, average, mean and projected mass estimators as described in Heisler et al. 1985 were used. The mass estimate within $0.5 h^{-1}\text{Mpc}$ for *group 2* is reported so as to compare with the Rosat X-ray estimate of Jones 1996. Good agreement within the errors is found for the average and median mass estimators. The mass for $R < 2.3\text{Mpc}$ is also shown (the limit of this survey) as a rough comparison with the X-ray estimate of Abramopoulos & Ku 1983 (Table 5) who reach a radius of $1.93 h^{-1}\text{Mpc}$ and whose value is far above the higher error bar on

all four mass estimators determined from the data in this paper. This is likely due to the fact that Abramopoulos & Ku 1983 used a β (the value of the dimensionless temperature) of 1, whereas other studies (Jones & Forman 1984) have since pointed to values between 0.5 and 0.7 for most clusters of galaxies.

In Table 5 calculated masses are also shown for subgroups 1 and 3. As noted in section 5.1.1 these groups are not likely to be virialized. This is because they are being tidally disrupted by the gravitational field of the main cluster group which would distort their distribution and prevent one from obtaining an accurate estimate of the mass using the virial theorem. Nonetheless the numbers are printed here for comparison with any future estimates.

5.2. Abell 133

5.2.1. 1D tests

ROSTAT and 3σ iterative clipping were employed to keep 120 velocities in the range $15279 < v < 18846$ km sec⁻¹. Table 3 shows the 90% confidence intervals about the location (C_{BI}) and scale (S_{BI}) of the 3 S_{BI} clipped data using 10000 bootstraps.

Table 3 also presents the results of the shape estimators on the velocity distribution (see figure 10a). Of the 4 estimators only the large kurtosis value would lead one to believe the distribution is non-Gaussian. The kurtosis implies the distribution is heavily tailed and that one should run KMM to look for in-falling groups along the line of sight. Attempts to identify two, three, four and five groups all failed with large margins. No multi-group fit came back with a null rejection of the single Gaussian hypothesis.

Given the failure of KMM to discern any multiple Gaussian structure one must look to the Z_{score} , 2D and 3D tests for any confirmation of the kurtosis.

5.2.2. *cD velocity offset, Z_{score}*

Table 4 shows the Z_{score} and cD peculiar velocity for Abell 133. There is a case for a “speeding cD” given the fact that the Z_{score} value with error does *not* bracket zero. Given that no possible host subclumps have been objectively verified one must assume this an indicator of dynamical youth. See the VDP section below for more.

5.2.3. *2D and 3D tests*

Table 4 also presents the 2D and 3D results using the 120 galaxies within $3S_{BI}$. Note that the centroid of the galaxy positions was taken as the center of the cluster. This was justified by the Z_{score} value indicating the cD is not at the center of the cluster, and therefore not a good place to pick the cluster center. It is important to pick a good center as some of the substructure indicators are sensitive to this value.

The Lee statistic has a small p value of 15. This indicates that a two group fit versus one is likely. Recall again that a p value of less than 25 indicates a statistically significant probability. Figure 10b shows a plot of the Lee distribution with a peak at 93.6° .

The lack of multiple peaks and the high value of L_{RAT} (Table 4) continue to insist that no more than two groups are likely in the X-Y plane. The Lee statistic was also run on the inner $1.5 h^{-1}\text{Mpc}$ region so as to compare with the AKM and Rosat data below. There were two peaks in the Lee distribution implying more complex structure as mentioned. One peak was at 88° which corresponds to the elongation seen in the AKM and Rosat maps (see section 5.2.6).

The other 3D estimators should verify this 2-D structure if it exists. While these estimators are not proficient at LOS substructure (which, outside the Kurtosis and Lee results, the 1D tests and KMM failure have ruled out) they are sensitive to 2D structure

in the plane of the sky. Table 4 contains the values for the Δ , α , and ϵ tests. Only the Δ statistic indicates a statistically significant level of substructure, in keeping with the Lee statistic. However, again it should be kept in mind that the Δ is the most optimistic, or most likely to give a false positive of the three.

5.2.4. *Rotation*

Figure 11a shows the C_{BI} velocities and their 90% confidence intervals binned along the elongation axis as given by the Lee statistic. There are no clear gradients which would indicate rotation.

This further emphasizes the Δ statistic result above. If one did see signs of rotation this might show up as a positive substructure result in the Δ test where small values of V_{rot}/σ may cause detection by the 3-D diagnostics. Since there are no signs of rotation in C_{BI} one can put more confidence in the Δ statistic result.

However there are discontinuities at -1 and 1.25 h^{-1} Mpc. The discontinuity at -1 may be explained by the low number of galaxies in the last two bins and the lack of sample south of 1.5 h^{-1} Mpc.

5.2.5. *Velocity Dispersion Profile (VDP)*

As for Abell 119 variations in the velocity dispersion were tested by plotting velocity versus radius (the caustics) in figure 11b and cumulative S_{BI} in figure 11c. Both plots are fairly flat out to 2.5 h^{-1} Mpc as in *group 2* of Abell 119. The flat VDP within 1 h^{-1} Mpc is again an indicator of galaxy velocity anisotropies and is supported by our Z_{score} result for Abell 133.

5.2.6. *Rosat versus AKM*

Figures 12a and 12b show the AKM and Rosat contour optical overlays for a 1.5×1.5 h^{-1} Mpc region centered on the central cD. These are once again restricted to the inner 1.5 Mpc since that is the extent to which one can gain meaningful information from the X-ray data at this distance.

The Rosat X-ray data has been smoothed with a 2 pixel FWHM Gaussian using the `imsmooth` task in the PROS X-ray reduction package. As above, the image was obtained from the publically released HEASARC Rosat CD Volume 2 (Corcoran et al. 1994).

If one focuses on the inner regions one can discern a slight NNE SWW elongation of the X-ray gas and galaxy distribution. As one goes farther away from the center the contours push out to the SE in both maps. This is in agreement with the elongation seen in the Lee statistic result for data within $1.5 h^{-1}$ Mpc. As well there appears to be small structures, again supported by the flat VDP.

5.2.7. *Radio*

Abell 133 has been reported as a strong radio source and studied by several groups (Slee et al. 1989, Owen et al. 1993, Gregorini et al. 1994). The radio structure of the cD has been resolved into two sources by Owen et al. 1993 (figure 1), but the orientation of the double structure does not correspond to the elongation axis of the cluster. The wide area radio map by Slee et al. 1989 (figure 9) also resolves the multiple cD components, but otherwise has no correspondence with the elongation angle of the cluster. As for Abell 119 if the cluster had formed recently one might expect to find the radio structure mimicking the larger scale structure, but since this is not the case it is presented as evidence of an older system with little substructure.

5.2.8. Mass

Table 5 compares this paper’s mass estimate for Abell 133 with the X-ray mass estimates of Jones 1996 for $R < 0.5h^{-1}\text{Mpc}$ and $R < 1.5h^{-1}\text{Mpc}$. For $R < 0.5h^{-1}\text{Mpc}$ all four mass estimates are in agreement with the X-ray data within their respective 90% confidence intervals. For $R < 1.5h^{-1}\text{Mpc}$ of the four estimators only the projected mass estimator (PME) does not overlap with the X-ray value. This is quite a surprising result given the substructure seen in the Rosat image in combination with the Lee, Δ , Z_{score} , and VDP results suggesting a system non-ideal for virial estimates of mass.

6. Discussion

Starting with 174 galaxies in Abell 119, which include this paper’s newly recorded velocities and those obtained from the literature, 3 sigma iterative clipping left 155. From the 1-D velocity distribution the ROSTAT statistical program yielded a high positive kurtosis in the remaining 155 galaxies pointing to tails heavier than expected for a Gaussian distribution. Subsequently the KMM partitioning algorithm was used to search for overlapping Gaussian distributions in the velocity field. Three overlapping distributions were found rejecting the single Gaussian distribution at the 97.9% confidence level. A main group of 125 members and two smaller groups of 11 and 17 were found. Further 1-D analysis with ROSTAT on the main subgroup of 125 members (*group 2*) lent support to a Gaussian distribution of velocities, while this was not the case for the 2 smaller sub groups. As well, the central galaxy was not significantly offset from the mean velocity of the cluster in *group 2* implying the lack of a speeding cD. The 2-D Lee statistic did not detect two groups in *group 2*, but did lend support to an elongation axis near 82.8° . Of the 3-D tests used on *group 2* only the Delta test was positive, but it should be noted that it is the more likely to detect a false positive of the 3-D estimators. No clear gradients were found in the

velocity field of *group 2*, further supporting the delta statistic which is susceptible to such gradients. The flat velocity dispersion profile for *group 2* points to velocity anisotropies in the central region. Rosat X-ray data was compared with the number density of galaxies in *group 2* as plotted using an Adaptive Kernel Map (AKM) within $1.5h^{-1}\text{Mpc}$ of the central cD galaxy. The elongation pointed out with the Lee statistic is replicated in both the Rosat and AKM maps implying that if one obtains enough galaxy redshifts in a cluster one can accurately begin to estimate the local matter density with confidence. Virial mass estimates of Jones 1996 from Rosat data compare nicely with those obtained from the velocity data presented here for those galaxies within $1.5h^{-1}\text{Mpc}$ of the central galaxy of *group 2*.

In Abell 133 a dynamical analysis using newly collected velocity data in combination with that of the literature was done starting with 153 velocities. 3 sigma iterative clipping reduced the 153 to 120. The remaining 1-D velocity data was analyzed with ROSTAT to yield a relatively high positive kurtosis, but when KMM was used to search for multiple Gaussian fits none were found with a significance level higher than that of a single Gaussian. However, the central cD galaxy was significantly offset from the cluster mean velocity which is an indicator of dynamical youth especially since there appears no host subclump for the central cD galaxy. This is further supported by the flat velocity dispersion profile seen in the inner part of the cluster implying velocity anisotropies. The Lee statistic was positive for a 2 group fit, but of the 3-D statistical indicators only the delta statistic supported the finding. However the delta statistic result itself was further supported by the lack of velocity gradients in the C_{BI} velocities along the elongation axis found with the Lee statistic. The Lee statistic run on the inner $1.5h^{-1}\text{Mpc}$ gives an elongation axis at 88° , which corresponds to what is seen in the Rosat and AKM images. The Lee statistic run on this portion of the data does show multiple peaks indicating more complex structure, also supported by what is seen in the Rosat image. The complex structure found above is again bolstered by the flat VDP seen, indicating velocity anisotropies in the inner regions of the cluster. All 4

mass estimates agree with the exception of the one for the projected mass estimator within $R < 1.5 h^{-1} \text{Mpc}$. This is quite a surprising result given the substructure seen in the Rosat image in combination with the Lee, Δ , Z_{score} , and VDP results which suggest a system non-ideal for virial estimates of mass. This can only be disentangled in the future by further velocity measurements in the field of this cluster.

Both of these X-ray clusters seem to demonstrate virialization to large radii given the good correlation between the X-ray and velocity mass estimators. However the Lee statistic for both of these clusters points to an elongation of the cluster. In Abell 133 a hint at two groups in the plane of the sky is also observed. In Abell 119 the elongation is less pronounced than that of Abell 133 where within $1 h^{-1} \text{Mpc}$ the distribution of galaxies gives one the qualitative impression of a small group falling toward the cD galaxy. The X-ray gas in this region of Abell 133 is also elongated in the center as can be seen in figure 12b. The situation for Abell 133 seems much more clear than that of Abell 119. Most of the indicators point to substructure in Abell 133, whereas in Abell 119 the results are more mixed. In either case it is clear that when substructure is taken into account via the statistical methods demonstrated within this paper the velocity+spatial versus X-ray virial estimators can compare nicely.

The authors would like to thank the Director of the Observatories of the Carnegie Institution of Washington for generous allocation of telescope time at Las Campanas. It is a pleasure to thank Steve Sackett for use of the spectrograph and P. Harding and John Filhaber for help with instrument setup. We would also like to thank Ricardo Flores and Tina Bird for useful discussions and the use of various programs. This research has made use of the NASA/IPAC Extragalactic Database (NED) which is operated by the Jet Propulsion Laboratory, California Institute of Technology, under contract with the National Aeronautics and Space Administration. As well, This research has made use of data

obtained through the High Energy Astrophysics Science Archive Research Center Online Service, provided by the NASA/Goddard Space Flight Center. This project was partially supported by FONDECYT grants 1960413 and 8970009. M.J. Way has been supported by Research and Research Board awards at The University of Missouri–St.Louis.

REFERENCES

- Abramopoulos, F. & Ku, W. 1983, ApJ 271, 446
- Ashman, K.M., Bird, C.M., & Zepf, S.E. 1994, AJ 108, 2348
- Beers, T.C., Flynn, K., & Gebhardt, K. 1990, AJ 100, 32
- Beers, T.C., Forman, W., Huchra, J.P., Jones, C., & Gebhardt, K. 1991, AJ102, 1581
- Bird, C. 1994 AJ 107, 1637
- Bird, C. 1993, Ph.D thesis, University of Minnesota and Michigan State University
- Bird, C., & Beers, T.C. 1993, AJ 105, 1596
- Chandrasekhar, S. 1943, ApJ97, 255
- Corcoran, M.F., O’Neel, B., Perry, K., Smale, W., White, N., & Petre, R. 1994 Rosat: The Images Volume 2 (HEASARC)
- de Vaucouleurs, G., de Vaucouleurs, A., Corwin, H., Buta, R., Paturel, G., & Fouque, P. 1991 Third Reference Catalogue of Bright Galaxies (Springer, New York)
- den Hartog, R. and Katgert, P. 1996, MNRAS 279, 349
- Dressler, A. & Schectman, S. 1988 AJ 95, 985
- Fadda, D., Girardi, M., Giuricin, G., Mardirossian, F., & Mezzetti, M. 1996 ApJ 473, 670
- Fabricant, D., Kurtz M., Geller M., Zabludoff A., Mack P., Wegner G. 1993 AJ 105, 788
- Fitchett, M.J. 1988 MNRAS 230, 169
- Gebhardt, K. & Beers, T.C. 1991 ApJ 383, 72

- Gregorini, L., de Ruiter, H.R., Parma, P., Sadler, E.M., Vettolani, G. & Ekers, R.D. 1994
A&AS 106, 1
- Heisler, J., Tremaine, S. & Bahcall, J.N. 1985, ApJ 298, 8
- Huchra, J., Davis, M., Latham, D., & Tonry, J. 1983 ApJS 52, 89
- Jacoby, G.H., Hunter, D.A. & Christian, C.A. 1984 ApJS 56, 257
- Jones, C. private communication
- Jones, C. & Forman, W. 1984 ApJ 276, 38
- Kaiser, N. 1987 MNRAS, 227, 1
- Kinman, T. & Hintzen, P. 1981 PASP, 93, 405
- M.J. Kurtz, D.J. Mink, W.F. Wyatt, D.G. Fabricant, G. Torres, G.A. Kriss, and J.L. Tonry
1991 in Astronomical Data Analysis Software and Systems I, ASP Conf. Ser., Vol.
25, eds. D.M. Worrall, C. Biemesderfer, and J. Barnes, p. 432-438.
- Malumuth, E., Kriss, G.A., Dixon, W.V.D., Ferguson, H.C. & Ritchie, C. 1992 AJ 104, 495
- Melnick J. & Quintana, H. 1981 AJ 86, 1567
- Merrifield, M. R., & Kent S. M. 1989 AJ 89, 351
- Owen, F.N., White, R.A., & Ge, J. 1993 ApJS 87, 135
- Pickles, A. J. 1985 ApJ 296, 340
- Quintana, H. & Lawrie 1982 AJ 87, 1
- Quintana, H., Ramirez, A. & Way, M.J. 1996 AJ 112, 36
- Sandage 1978 AJ 83, 904

- Shectman S., Carnegie Institution of Washington Year Book 1989, p.25-32
- Slee, O.B., Perley, R.A. & Siegman, B.C. 1989 Aust J. Phys. 42, 633
- Tody, D. 1993, "IRAF in the Nineties" in Astronomical Data Analysis Software and Systems II, A.S.P. Conference Ser., Vol 52, eds. R.J. Hanisch, R.J.V. Brissenden, and J. Barnes, 173.
- Tonry, J. & Davis, M. 1979 AJ 84, 1511
- West, M.J. & Bothun, G.D. 1990, ApJ 350, 36
- Yahil, A., & Vidal, N.V. 1977, ApJ 214, 347
- Zabludoff, A., Geller, M., Huchra, J. & Vogeley, M. 1993, AJ 106, 1273
- Zhao, J., Burns, J.O., & Owen, F.N. 1989, AJ 98, 64

Fig. 1.— X-Y positions for galaxies in Abell 119 picked from the ESO Quick Blue survey plates.

Fig. 2.— X-Y positions for galaxies in Abell 133 picked from the ESO Blue plates.

Fig. 3.— Velocity residuals between Abell 133 and 119 in this paper and Melnick & Quintana 1981. A 0th order Polynomial line was fit for those values within 3.0σ of the mean.

Fig. 4.— Velocity between Abell 133 and 119 in this paper and Fabricant et al. 1993. Same line fitting technique as used in Figure 2a.

Fig. 5.— Velocity histogram of Abell 119 for the 153 galaxies within $3S_{BI}$.

Fig. 6.— Velocity histogram of Abell 119 Group 2.

Fig. 7.— Three groups from the $3S_{BI}$ clipped Abell 119 data partitioned with KMM. Group 1 is denoted by \square (11 members), group 2 by \bullet (125 members) and group 3 by $+$ (17 members).

Fig. 8.— Lee statistic for Abell 119, $LRAT = 2.231374$, $N_{gal} = 153$.

Fig. 9.— Lee statistic for Abell 119 group 2, $LRAT = 1.5829$, $N_{gal} = 125$.

Fig. 10.— Abell 119 $C_{BI}(R)-C_{BI}(\text{global})$ versus R . There is no clear gradient in the data implying a lack of any clearly definable rotation.

Fig. 11.— Abell 119 Group 2 $C_{BI}(R)-C_{BI}(\text{global})$ versus R . Once again there is no clear gradient in the data implying a lack of any clearly definable rotation.

Fig. 12.— Caustics for Abell 119 (153 galaxies).

Fig. 13.— Caustics for Abell 119 Group 2 (125 galaxies).

Fig. 14.— Abell 119: Binned cumulative S_{BI} versus R . (153 galaxies).

Fig. 15.— Abell 119 Group 2: Binned cumulative S_{BI} versus R . (125 galaxies).

Fig. 16.— Abell 119 Rosat X-ray - optical map overlay within $R < 1.5h^{-1}\text{Mpc}$.

Fig. 17.— Abell 119 Group 2 Adaptive Kernel - optical map overlay within $R < 1.5h^{-1}\text{Mpc}$.

Fig. 18.— Abell 133 Velocity Histogram for the 120 galaxies within $3S_{BI}$.

Fig. 19.— Lee statistic for Abell 133. $\text{LRAT} = 2.415$

Fig. 20.— Abell 133 $C_{BI}(R) - C_{BI}(\text{global})$ versus R . There is no clear gradient in the data implying a lack of any clearly definable rotation.

Fig. 21.— Caustics for Abell 133.

Fig. 22.— Abell 133: Binned cumulative S_{BI} versus R .

Fig. 23.— Abell 133 Rosat X-ray - optical map overlay within $R < 1.5h^{-1}\text{Mpc}$.

Fig. 24.— Abell 133 Adaptive Kernel - optical map overlay within $R < 1.5h^{-1}\text{Mpc}$.

TABLE 1. A119 - Velocities

Ident.	α (1950)	δ (1950)	v_{\odot}	err	R	Ref	Id.Ref	\bar{v}_{\odot}	err
25007	0 50 25.9	-02 03 29.6	13586	66	4.5	fi			
25003	0 50 39.1	-01 04 16.2	40924	76	3.9	fi			
25005	0 50 46.8	-01 34 08.5	13148	45	6.2	fi			
25012	0 50 55.9	-00 56 53.8	13089	70	3.5	fi			
25024	0 51 08.1	-02 12 05.0	13782	29	10.1	fi			
25020	0 51 09.2	-01 21 22.2	13027	42	6.1	fi			
25015	0 51 12.7	-01 03 04.5	41345	57	4.9	fi			
25017	0 51 13.4	-01 09 14.7	14173	38	7.9	fi			
25018	0 51 14.4	-01 11 41.9	14082	89	2.4	fi			
25027	0 51 18.4	-02 11 16.3	20624	89	3.9	fi			
25031	0 51 25.7	-01 32 21.7	16058	50	6.1	fi			
25030	0 51 25.7	-01 43 26.0	13083	48	6.4	fi			
25040	0 51 37.5	-02 13 25.1	13480	39	8.7	fi			
25038	0 51 38.8	-01 41 57.8	13060	32	8.8	fi			
25035	0 51 41.3	-00 55 33.0	43573	130	2.9	fi			
25045	0 51 42.2	-02 04 04.7	13813	51	4.3	fi			
25047	0 51 42.6	-01 30 36.9	13506	31	8.7	fi			
25049	0 51 52.7	-01 11 56.5	12742	39	7.0	fi			
25057	0 52 05.5	-01 50 42.0	12666	42	6.0	fi			
25058	0 52 07.7	-01 50 44.3	12464	37	7.5	fi		12481	30
			12534	44		FAB93	8		
25065	0 52 08.6	-01 23 39.6	15944	53	5.1	fi			
25062	0 52 08.9	-01 45 35.9	11910	41	6.9	fi		11875	32
			11873	38		FAB93	20		
25064	0 52 16.1	-01 39 33.8	13989	31	9.5	fi		13990	30
			14021	55		FAB93	25		
25063	0 52 17.4	-01 45 00.4	13889	37	7.9	fi		13905	30
			13959	46		FAB93	19		
25061	0 52 20.2	-01 50 50.6	13995	31	8.5	fi		14048	67
			14160	39		FAB93	7		
25076	0 52 22.5	-01 43 24.6	29368	50	4.9	fi		29381	45
			29462	100		FAB93	21		
25078	0 52 23.5	-01 57 29.2	30284	98	5.1	fi			
25077	0 52 23.9	-01 51 19.6	32394	61	4.8	fi			
25079	0 52 25.5	-02 09 06.3	13681	45	6.8	fi			
25075	0 52 30.2	-01 35 17.1	13883	92		FAB93	56		
25073	0 52 31.7	-01 31 23.6	13011	27	10.1	fi			
25072	0 52 32.2	-01 30 15.8	13351	56		FAB93	70		
25070	0 52 35.5	-01 19 00.8	13777	26	10.9	fi		13742	81
			13600	60		MQ81	23		
25092	0 52 37.8	-01 04 50.5	13663	36	7.6	fi			
25088	0 52 40.3	-01 20 46.8	14569	80	6.7	fi			
25090	0 52 43.5	-01 11 18.5	13242	32	9.1	fi			
25086	0 52 44.6	-01 33 24.8	13546	46	1	fi		13532	33
			13546	46		FAB93	55		
25085	0 52 45.2	-01 35 19.3	14166	84		FAB93	53		
25087	0 52 45.5	-01 32 52.1	13427	30	11.7	fi		13405	36
			13390	50		MQ81	4		

TABLE 1. (continued)

Ident.	α (1950)	δ (1950)	v_{\odot}	err	R	Ref	Id.Ref	\bar{v}_{\odot}	err
25083	0 52 48.0	-01 37 23.3	12490	42	7.0	fibr			
25099	0 52 49.6	-01 28 53.8	12577	56	5.0	fibr		12594	42
			12645	65		FAB93	69		
25105	0 52 51.9	-01 34 45.6	12472	27	12.1	fibr		12462	30
			12462	45		FAB93	51		
25094	0 52 52.3	-01 00 45.5	13356	42	6.7	fibr			
25098	0 52 56.1	-01 24 11.4	11887	26	11.6	fibr		11887	26
			19235	300		MQ81	20		
25107	0 52 57.2	-01 41 04.8	12873	34	9.7	fibr		12868	30
			12890	39		FAB93	24		
25093	0 52 58.2	-00 48 02.3	13963	54	5.7	e fibr			
25096	0 52 58.3	-01 17 37.4	34667	47	5.8	fibr			
25100	0 52 58.9	-01 28 53.7	13810	44	5.3	fibr			
25119	0 53 04.9	-01 51 00.5	14692	49	6.8	fibr			
25122	0 53 06.6	-01 45 34.6	12845	36	9.0	fibr			
25126	0 53 07.3	-01 34 58.0	13017	35	7.8	fibr		13033	30
			13092	48		FAB93	50		
25137	0 53 09.7	-01 18 15.2	12655	32	7.7	fibr		12658	30
			12694	48		FAB93	91		
25129	0 53 11.5	-01 29 11.1	12529	51	4.4	fibr			
25125	0 53 11.9	-01 35 42.0	13770	31	9.5	fibr		13746	41
			13705	52		FAB93	49		
25111	0 53 13.2	-02 07 21.3	13190	58	4.8	fibr			
25116	0 53 14.5	-01 58 24.0	12857	45	5.7	fibr		12906	47
			12980	44		FAB93	1		
25134	0 53 16.2	-01 21 07.5	13411	32	8.7	fibr			
25148	0 53 17.7	-01 26 06.0	14385	47	6.2	fibr		14330	48
			14316	41		FAB93	76		
25159	0 53 18.9	-01 46 20.1	13104	33	9.3	fibr		13118	30
			13172	44		FAB93	18		
25144	0 53 20.1	-01 10 16.6	13247	31	9.6	fibr		13282	90
			13560	80		MQ81	17		
25146	0 53 20.8	-01 11 35.0	13294	39	7.6	fibr		13268	33
			13270	50		MQ81	9		
25145	0 53 21.1	-01 11 25.7	13633	43	7.8	fibr		13676	70
			13835	70		MQ81	8		
25151	0 53 22.3	-01 31 03.0	12179	40	8.5	fibr		12189	30
			12190	33	10.6	fibr			
			12320	130		MQ81	5		
25154	0 53 25.7	-01 34 14.6	14697	39	9.1	fibr		14692	30
			14712	48		FAB93	47		
25163	0 53 28.6	-01 49 12.7	12705	40	7.1	fibr		12717	37
			12827	106		FAB93	15		
25157	0 53 29.3	-01 36 16.9	12795	30	11.2	fibr			
99999	0 53 30.0	-01 35 00.0	12851	73		ZAB93			
25143	0 53 29.8	-01 05 53.8	13408	29	10.3	fibr			
25165	0 53 30.0	-02 12 06.3	4048	25	5.0	e fibr			
25201	0 53 31.8	-00 43 30.8	12895	53	5.0	fibr			

TABLE 1. (continued)

Ident.	α (1950)	δ (1950)	v_{\odot}	err	R	Ref	Id.Ref	\bar{v}_{\odot}	err
25191	0 53 32.5	-01 19 38.9	12949	41	6.5	fibr		12935	35
			12928	64		FAB93	87		
25170	0 53 33.7	-01 36 49.2	13844	29	10.3	fibr		13836	30
			13836	54		FAB93	36		
25175	0 53 36.9	-01 32 16.6	13690	56		FAB93	67		
25187	0 53 37.0	-01 24 37.7	14517	29	9.4	fibr		14516	30
			14540	50		FAB93	82		
25190	0 53 37.3	-01 23 13.7	12497	36	8.7	fibr		12501	33
			12565	80		MQ81	11		
25166	0 53 38.0	-01 48 06.0	14741	37	8.1	fibr		14736	30
			14758	42		FAB93	14		
25199	0 53 38.9	-00 50 44.5	13230	70	3.5	fibr			
25186	0 53 40.9	-01 24 52.2	13491	30	9.0	fibr		13476	30
			13452	56		FAB93	81		
25180	0 53 42.7	-01 31 32.3	13326	35	10.1	fibr		13282	38
			13320	100		MQ81	1		
			13246	45		RC3			
25220	0 53 42.9	-01 35 01.9	12693	47	5	e fibr		12711	30
			12752	40		FAB93	45		
25229	0 53 43.1	-01 48 48.6	13109	46	7.6	fibr		13125	31
			13166	41		FAB93	13		
25207	0 53 43.6	-01 13 24.6	42012	48	7.0	fibr			
25179	0 53 44.4	-01 31 50.1	11712	41		FAB93	64		
25178	0 53 44.5	-01 31 56.5	11554	86		FAB93	63		
25181	0 53 44.8	-01 30 43.3	13131	36	9.4	fibr		13129	30
			13170	50		MQ81	15		
25188	0 53 45.0	-01 24 17.2	11061	48		FAB93	80		
25213	0 53 47.6	-01 26 48.1	11730	34	8.8	fibr		11717	60
			11480	160		MQ81	12		
25227	0 53 48.5	-01 43 11.0	13933	44	5.6	fibr			
25214	0 53 49.5	-01 28 47.8	14945	29	11.3	e fibr		14873	175
			14705	50		MQ81	3		
25208	0 53 50.1	-01 15 25.4	13179	43	11.4	fibr		13185	39
			13255	90		MQ81	16		
25212	0 53 51.2	-01 24 47.5	12886	31	9.8	e fibr		12839	77
			12760	50		MQ81	13		
25217	0 53 52.2	-01 31 57.1	11434	31	10.4	fibr		11456	30
			11575	250		MQ81	2		
			11541	48		RC3			
25233	0 53 52.2	-02 05 02.7	13866	43	6.0	fibr			
25218	0 53 52.5	-01 32 42.6	13041	44	7.7	fibr		12995	80
			12765	80		MQ81	14		
			13069	49		FAB93	44		
25230	0 53 53.2	-01 53 46.5	13706	37	8.4	fibr		13731	41
			13826	61		FAB93	5		
25206	0 53 53.9	-01 03 45.0	12948	46	4.9	fibr			
25225	0 53 54.6	-01 42 19.9	13458	32	9.3	fibr		13467	32
			13607	111		FAB93	23		

TABLE 1. (continued)

Ident.	α (1950)	δ (1950)	v_{\odot}	err	R	Ref	Id.Ref	\bar{v}_{\odot}	err
25216	0 53 55.8	-01 29 49.1	11404	100		FAB93	59		
25241	0 53 57.1	-01 48 15.1	14461	29	9.8	fibr			
25251	0 53 57.3	-01 26 35.2	12657	29	10.0	fibr		12655	30
			12678	41		FAB93	74		
25239	0 53 58.1	-01 53 12.0	13586	71		FAB93	4		
25245	0 53 58.2	-01 37 54.9	12766	35	7.4	fibr		12758	32
			12750	76		FAB93	33		
25237	0 53 59.3	-02 2 32.5	3970	100		MQ81	21	4006	30
			4010	22		HDTL			
25250	0 54 02.3	-01 32 08.7	13248	57	5.5	fibr			
25257	0 54 02.4	-00 48 04.2	13258	61	4.1	fibr			
25240	0 54 03.9	-01 48 36.8	13127	39	6.7	fibr		13142	36
			13247	88		FAB93	11		
25253	0 54 05.0	-01 23 46.3	13535	33	7.9	fibr			
25244	0 54 05.2	-01 39 38.2	13187	30	10.1	fibr		13198	42
			13386	114		FAB93	31		
25246	0 54 05.3	-01 37 19.1	13383	36	8.8	fibr		13380	30
			13399	57		FAB93	32		
25248	0 54 05.7	-01 33 55.4	15211	56	4.6	e fibr		15079	150
			15022	45		FAB93	43		
25242	0 54 06.4	-01 44 42.3	12908	28	10.0	fibr			
25254	0 54 07.5	-01 18 16.5	13313	49	6.6	fibr		13270	38
			13265	43		FAB93	86		
25263	0 54 11.1	-01 08 41.5	14064	34	8.8	fibr		14057	30
			14068	55		FAB93	108		
25281	0 54 12.8	-01 48 51.5	12034	35	9.0	fibr			
25275	0 54 13.0	-01 33 03.5	12610	30		FAB93	42		
25282	0 54 13.3	-01 52 00.7	13456	41	6.2	fibr		13504	71
			13638	61		FAB93	3		
25262	0 54 13.6	-01 08 53.1	13059	40	8.0	fibr			
25285	0 54 13.9	-02 03 22.2	12391	65	3.8	e fibr			
25258	0 54 15.9	-00 53 44.3	13772	35	6.9	fibr			
25274	0 54 18.1	-01 32 33.0	12245	30	11.1	fibr		12256	30
			12299	34		FAB93	41		
25271	0 54 19.3	-01 25 44.8	13748	28	9.3	fibr		13724	30
			13689	74	3.0	fibr			
			13699	47		FAB93	72		
25266	0 54 23.0	-01 12 48.6	12791	42	7.1	fibr			
25280	0 54 23.4	-01 43 23.1	13848	57	4.9	fibr			
25273	0 54 23.5	-01 28 54.0	14964	76	2.9	e fibr		15029	36
			15048	41		S78			
25289	0 54 23.7	-01 39 31.9	13091	33	8.3	fibr			
25290	0 54 24.9	-01 38 58.1	14806	42	6.4	fibr			
25294	0 54 25.2	-01 31 37.1	13523	80		FAB93	57		
25301	0 54 26.8	-01 05 42.8	14589	70	4.1	e fibr			
25303	0 54 27.9	-01 01 33.1	12984	50	5.8	fibr			
25298	0 54 28.5	-01 08 59.4	13913	27	10.5	fibr		13911	30
			13935	39		FAB93	106		

TABLE 1. (continued)

Ident.	α (1950)	δ (1950)	v_{\odot}	err	R	Ref	Id.Ref	\bar{v}_{\odot}	err
99999	0 54 28.7	-01 08 45.0	13535			RC3	3405		
25299	0 54 29.0	-01 08 42.4	13060	91	3.2	fibr			
25296	0 54 31.5	-01 11 20.5	13451	53	5.5	fibr		13377	52
			13369	37		FAB93	97		
25288	0 54 33.6	-01 40 03.0	14565	37	8.2	fibr			
25291	0 54 36.3	-01 39 00.9	12010	31	10.7	fibr			
25319	0 54 37.2	-01 17 19.2	12330	52	4.7	fibr		12393	108
			12625	90		MQ81	18		
25292	0 54 37.8	-01 39 00.1	14656	37	7.3	fibr		14651	32
			14665	62		FAB93	28		
25324	0 54 38.7	-02 01 42.5	23761	68	3.3	fibr			
25313	0 54 40.3	-00 55 01.9	12654	31	9.9	fibr		12666	76
			13200	200		MQ81	19		
25318	0 54 40.4	-01 16 54.7	11752	36	9.0	fibr		11752	36
			14765	230		MQ81	22		
25322	0 54 41.2	-01 33 20.5	12965	33	8.6	fibr		12963	30
			12988	41		FAB93	40		
25314	0 54 43.4	-00 56 21.8	13518	56	6.1	fibr		13636	105
			13775	50		MQ81	7		
25312	0 54 47.6	-00 54 08.7	22821	89	2.8	fibr			
25315	0 54 51.3	-01 00 36.0	18828	55	6.4	fibr		18793	38
			18788	53		FAB93	117		
25310	0 54 52.2	-00 47 22.8	12669	47	6.8	fibr			
25329	0 54 52.9	-01 36 48.3	13063	24	11.7	fibr		13076	63
			13411	117		FAB93	27		
25335	0 54 54.0	-00 44 28.7	13156	53	7.2	fibr			
25331	0 54 58.4	-01 11 51.6	13434	51		FAB93	96		
25328	0 55 01.5	-01 39 39.6	13533	42	7.8	fibr		13491	34
			13467	71		ZAB93			
			13465	60		MQ81	6		
25350	0 55 03.0	-02 08 02.1	23799	84	3.1	fibr			
99999	0 55 06.0	-01 38 00.0	13427			RC3	3444		
25344	0 55 06.4	-01 09 44.2	13761	32	8.8	fibr		13745	39
			13678	77		FAB93	103		
25341	0 55 06.6	-00 51 39.6	13680	66	3.7	fibr			
25347	0 55 08.3	-01 34 55.2	14219	67	2.8	e fibr			
25340	0 55 12.9	-00 51 07.0	13893	68	5.2	fibr			
25345	0 55 15.3	-01 16 25.3	12882	36	9.7	fibr			
25360	0 55 18.3	-01 24 20.5	13091	53	5.2	e fibr			
25361	0 55 20.2	-01 05 03.7	12651	47	5.4	fibr		12620	40
			12598	59		FAB93	111		
25352	0 55 29.4	-02 18 29.2	12814	41	6.8	fibr			
25362	0 55 31.6	-00 57 32.3	12694	64	3.8	fibr			
25374	0 55 44.6	-01 25 06.2	15647	38	10.2	fibr		15609	43
			15562	42	7.5	fibr			
25368	0 55 47.4	-02 12 23.7	13018	37	8.0	fibr			
25372	0 55 51.3	-01 39 51.0	15468	75	3.8	e fibr		15473	70
			15510	200		KH			

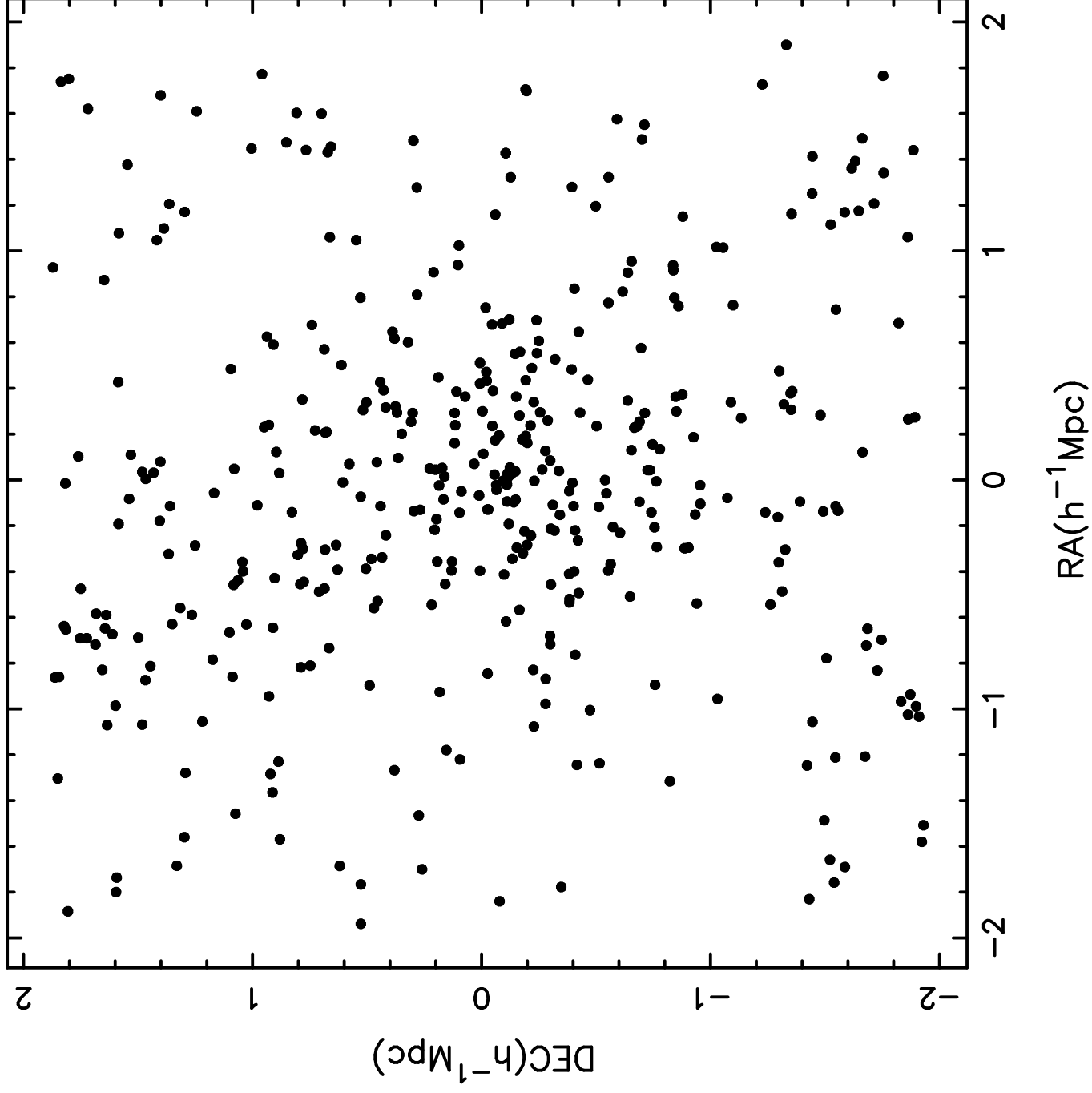
TABLE 1. (continued)

Ident.	α (1950)	δ (1950)	v_{\odot}	err	R	Ref	Id.Ref	\bar{v}_{\odot}	err
25370	0 55 51.5	-02 05 49.9	12661	42	7.8	fibr		12613	58
			12544	50	5.7	fibr			
25381	0 55 58.7	-01 50 20.3	12801	74	3.4	fibr			
25380	0 56 03.6	-01 05 28.0	22697	131	3	e	fibr		
25386	0 56 13.3	-01 01 16.5	13333	66	5.1	fibr			
25385	0 56 14.1	-01 21 59.5	13935	56	4.5	e	fibr	13939	40
			13942	56	6	e	fibr		
25389	0 56 24.9	-01 06 18.0	13631	34	7.8	fibr			
25392	0 56 34.1	-02 08 26.0	24554	47	5.9	fibr			
25393	0 56 37.4	-02 10 07.5	15582	77	3.6	e	fibr		
25400	0 56 42.2	-00 47 51.8	52499	95	3.3	fibr			
25398	0 56 45.2	-01 15 25.8	13690	36	7.9	fibr			

References for Table 1.

This paper: fibr = LCO fiber spectra; FAB93 = Fabricant et al. (1993); HDTL = Huchra et al. (1983); MQ81 = Melnick & Quintana (1981); KH=Kinman & Hintzen (1981); RC3 = de Vaucouleurs et al. (1991); S78 = Sandage (1978); ZAB93 = Zabludoff et al. (1993)

Abell 119 positions



Abell 133 positions

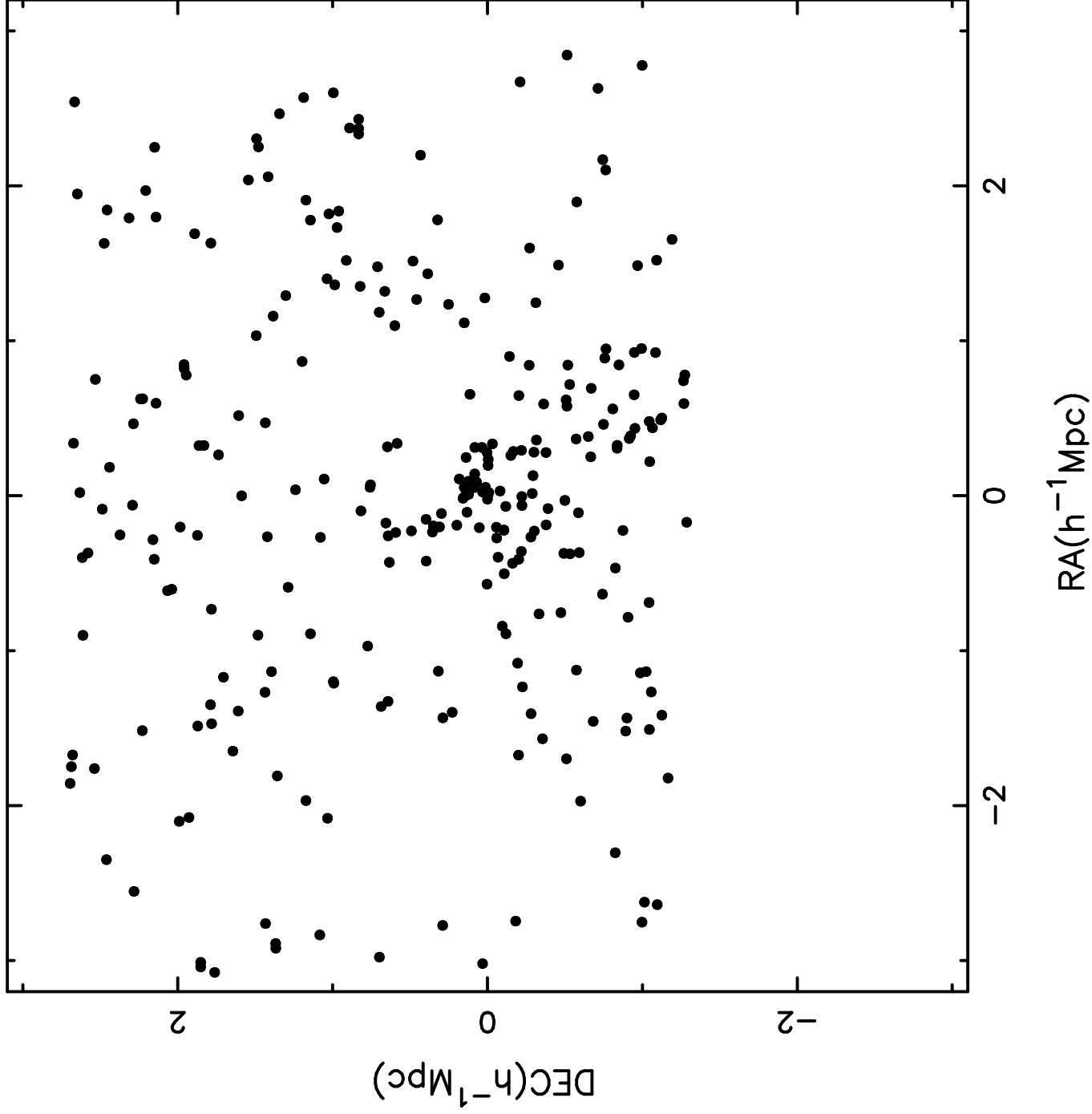


TABLE 2. A133 - Velocities

Ident.	α (1950)	δ (1950)	v_{\odot}	err	R		Ref	Id.Ref	\bar{v}_{\odot}	err
25022	0 57 10.1	-21 39 48.7	16587	52	4.8	e	fibr			
25025	0 57 29.8	-21 49 12.6	15952	49	5.7		fibr			
25026	0 57 31.5	-21 47 54.6	17433	46	6.4		fibr			
25024	0 57 34.9	-22 02 21.7	16400	50	5.7		fibr			
25027	0 57 35.0	-21 45 27.5	16734	40	9.5		fibr		16753	30
			16805				RC3	3582		
25035	0 57 39.3	-21 49 00.0	16459	51	3.9		fibr			
25033	0 57 42.8	-21 30 01.9	5635	46	7	e	fibr		5630	30
			5629	23	5	e	fibr			
25034	0 57 48.2	-21 32 11.3	18297	78	3.1	e	fibr			
25038	0 57 58.0	-22 31 31.2	55579	39	7.8		fibr			
25044	0 57 58.2	-21 50 13.7	16404	48	6.4		fibr			
25042	0 57 58.5	-21 59 06.1	16170	151	3		fibr			
25040	0 58 00.9	-22 18 27.3	16136	37	7.8		fibr			
25039	0 58 01.1	-22 28 59.2	17249	48	4.9		fibr			
25041	0 58 05.8	-22 01 03.0	25300	40	3	e	fibr			
25047	0 58 12.1	-21 48 40.7	34366	36	7.7		fibr			
25048	0 58 13.0	-21 52 04.0	17298	29	9.9		fibr		17307	30
			17325	40	8.0		fibr			
25045	0 58 18.4	-21 42 10.0	16505	38	7.0		fibr			
25050	0 58 20.5	-21 59 35.0	12536	32	10.4		fibr			
25054	0 58 23.4	-22 03 50.2	40375	92	2.9	e	fibr			
25056	0 58 27.9	-21 54 36.4	34675	54	5.2		fibr			
25057	0 58 30.1	-21 40 29.4	17245	39	7.2		fibr			
25053	0 58 34.0	-22 05 54.9	17680	40	6.7		fibr			
25055	0 58 35.6	-21 56 41.0	16926	44	6.6		fibr			
25058	0 58 41.3	-21 38 13.8	16692	36	7.8		fibr			
25059	0 58 48.9	-22 24 47.3	16593	37	7.5		fibr			
25062	0 58 50.9	-22 28 33.7	17632	84	3.0		fibr			
25061	0 58 51.1	-22 31 23.1	16942	29	10.0		fibr			
25068	0 58 53.3	-22 11 56.6	17005	37	6.8		fibr			
25065	0 58 54.3	-22 24 37.4	24804	29	4	e	fibr			
25069	0 58 56.2	-21 44 20.0	16853	29	9.2		fibr			
25070	0 58 57.9	-21 28 38.0	16472	38	7.8		fibr			
25064	0 58 58.1	-22 26 30.4	17475	32	8.7		fibr			
25066	0 58 58.2	-22 19 42.0	17435	41	6.6		fibr			
25067	0 58 58.3	-22 14 33.8	15776	64	5	e	fibr			
25071	0 59 00.1	-21 28 38.9	5500	97	3	e	fibr			
25084	0 59 07.2	-22 35 06.0	17120	51	4.6		fibr			
25081	0 59 09.3	-22 19 56.7	16020	36	11.2		fibr			
25082	0 59 11.6	-22 22 49.5	16770	38	7.6		fibr			
25077	0 59 15.0	-22 06 40.8	16322	27	9.5		fibr			
25083	0 59 15.2	-22 28 31.8	17407	49	4.8		fibr			
25078	0 59 15.7	-22 13 11.1	16327	113	3.0		fibr			
25074	0 59 17.6	-21 22 50.3	16652	50	6.6		fibr			
25075	0 59 17.6	-21 23 07.2	16625	42	7.0		fibr			
25079	0 59 20.6	-22 16 29.6	16093	32	7.5		fibr			
25085	0 59 20.3	-22 35 09.8	15603	31	5	e	fibr		15585	33

TABLE 2. (continued)

Ident.	α (1950)	δ (1950)	v_{\odot}	err	R		Ref	Id.Ref	\bar{v}_{\odot}	err
			15528	55	5	e	fibr			
25090	0 59 23.4	-22 25 40.7	15299	36	6.8		fibr			
25086	0 59 28.6	-22 32 13.2	15630	31	3	e	fibr			
25093	0 59 31.4	-21 39 26.1	16313	60	5.0		fibr			
25095	0 59 31.9	-21 21 53.2	30779	52	5.8		fibr			
25091	0 59 32.2	-22 24 27.4	16675	39	7.7		fibr			
25088	0 59 34.3	-22 30 58.6	17912	50	4.7	e	fibr			
99999	0 59 36.0	-19 43 06.0	16891	33			RC3	3695		
25112	0 59 39.2	-22 22 25.8	16403	58	4.7	e	fibr			
25115	0 59 40.4	-22 27 52.5	17492	27	11.3		fibr			
25111	0 59 40.6	-22 20 49.1	15619	104	3.4	e	fibr			
25100	0 59 43.2	-21 56 58.7	12479	43	6	e	fibr			
25113	0 59 44.2	-22 26 16.6	16839	41	7.8		fibr			
25097	0 59 44.4	-21 30 36.5	16797	52	6.3		fibr			
25098	0 59 44.4	-21 31 16.4	16482	77	5.0		fibr			
25101	0 59 45.5	-22 07 19.8	16719	84	2.4		fibr			
25102	0 59 45.5	-22 08 16.7	16315	39	7.2	e	fibr			
25105	0 59 47.8	-22 12 27.4	18132	34	8.9		fibr			
25107	0 59 47.2	-22 13 31.8	17216	149	2.7		fibr			
25108	0 59 48.2	-22 15 12.3	15837	36	8.4		fibr			
25103	0 59 48.3	-22 08 56.2	17216	44	7.4		fibr			
25110	0 59 48.4	-22 16 47.6	15555	64	3.5	e	fibr			
99999	0 59 50.0	-19 56 18.0	17927	30			RC3	3705		
25106	0 59 50.1	-22 12 07.8	16999	39	7.2		fibr			
25119	0 59 50.8	-22 22 45.5	17056	47	7.1		fibr			
25124	0 59 51.3	-22 06 09.4	17552	29	10.5		fibr			
25122	0 59 52.3	-22 09 07.3	17373	46	6.9		fibr			
25118	0 59 53.7	-22 30 36.0	16249	37	8.9		fibr			
25123	1 00 00.7	-22 07 18.2	16263	27	11.3		fibr			
25120	1 00 01.7	-22 15 04.8	16985	37	9.0		fibr			
25130	1 00 03.6	-21 47 16.9	17125	33	10.0		fibr			
25133	1 00 03.6	-22 05 15.0	16371	38	8.0		fibr			
25140	1 00 04.9	-22 06 27.8	16390	56	6.0		fibr			
25142	1 00 05.4	-22 07 33.1	12024	72	4.8		fibr			
25132	1 00 07.0	-21 53 26.1	28154	36	7.8	e	fibr			
25144	1 00 08.4	-22 08 44.7	16846	31	10.4		fibr		16856	30
			17053	80			MK			
25148	1 00 10.7	-22 10 42.0	15521	80			MK			
25147	1 00 11.0	-22 09 11.0	16885	80			MK			
25143	1 00 11.1	-22 08 22.8	15415	30	10.6		fibr			
25151	1 00 11.9	-22 14 58.7	16896	46	7.3		fibr			
25136	1 00 12.4	-22 06 30.7	16409	40	8.8		fibr			
25146	1 00 12.9	-22 09 04.7	17635	31	7.7		fibr		17629	30
			17722	80			MK			
25128	1 00 13.3	-21 36 17.3	16907	47	7.6		fibr		16976	78
			17064	53	5.6		fibr			
25149	1 00 13.7	-22 13 35.2	17481	36	9.3		fibr			
25134	1 00 14.7	-22 05 44.9	16462	33	8.3		fibr			

TABLE 2. (continued)

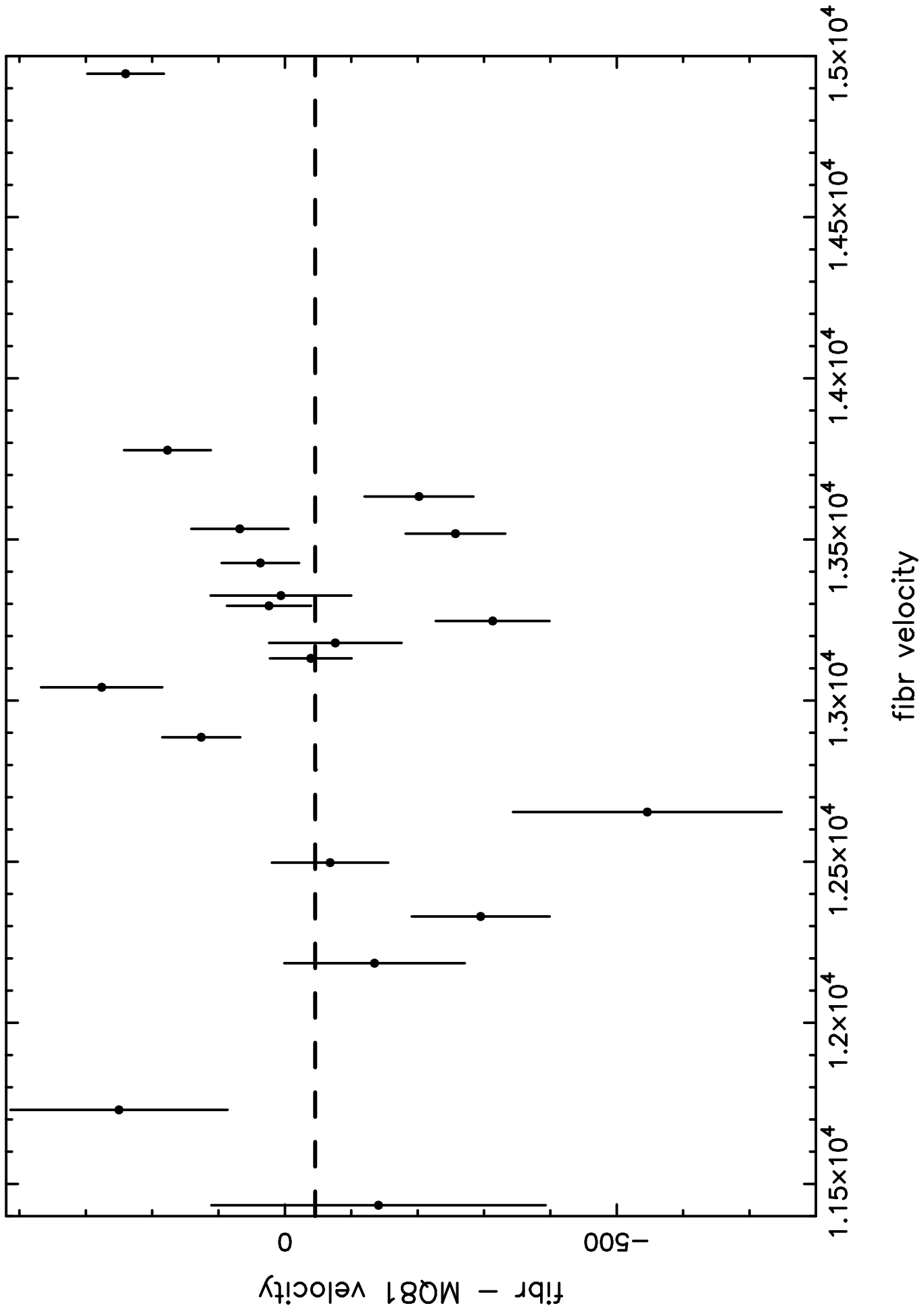
Ident.	α (1950)	δ (1950)	v_{\odot}	err	R	Ref	Id.Ref	\bar{v}_{\odot}	err
99999	1 00 15.7	-22 08 09.0	17551	80		MK			
25145	1 00 15.2	-22 09 01.2	17052	47	10.2	fibr		17051	30
			17089			RC3	3727		
			17160	100		MK			
99999	1 00 18.0	-22 38 00.0	35376			RC3	3730		
25150	1 00 18.8	-22 13 36.1	16953	25	12.0	fibr			
25157	1 00 19.3	-22 11 26.4	18475	47	7.3	fibr			
25171	1 00 21.9	-21 52 09.7	16566	33	9.2	fibr			
25167	1 00 26.8	-22 00 49.9	18326	39	7.4	fibr			
25153	1 00 28.4	-22 35 31.9	16488	38	7.8	fibr			
25170	1 00 28.9	-21 55 29.3	16206	42	6.3	fibr			
25155	1 00 29.9	-22 16 49.0	16746	24	11.1	fibr			
25158	1 00 31.3	-22 10 12.1	17224	46	7.4	fibr			
25190	1 00 33.1	-22 27 02.7	15555	39	8.4	fibr			
25182	1 00 33.4	-21 58 53.0	17195	43	6.6	fibr			
25168	1 00 34.3	-21 56 48.2	17474	42	7.9	fibr			
25179	1 00 36.0	-21 30 25.0	17860	99	3.2	e fibr			
25169	1 00 36.2	-21 55 48.1	16649	28	9.0	fibr			
25180	1 00 36.7	-21 39 42.9	15813	54	3.2	e fibr			
25181	1 00 37.1	-21 46 47.4	17500	37	8.4	fibr			
25178	1 00 38.5	-21 24 29.2	16022	58	4	e fibr			
25184	1 00 45.1	-22 13 30.7	15995	29	10.8	fibr		15985	30
			15961	45	5.6	fibr			
25189	1 00 45.9	-22 21 13.1	18307	30	10.1	fibr			
25187	1 00 46.3	-22 19 09.9	18062	31	8.8	fibr			
25188	1 00 46.5	-22 19 59.2	18405	42	8.8	fibr			
25198	1 00 49.7	-21 24 38.4	17716	62	5.1	fibr			
25196	1 00 50.7	-22 0 51.7	15961	69	4.1	fibr			
25201	1 01 05.8	-21 42 28.7	16172	45	5.3	fibr			
25200	1 01 06.9	-21 26 59.4	25883	50	5.4	fibr			
25199	1 01 07.7	-21 26 25.8	25970	65	5.3	fibr			
25203	1 01 09.7	-22 24 19.2	17420	45	6.8	fibr			
25204	1 01 14.5	-22 30 31.1	42414	63	4.2	fibr			
25210	1 01 18.4	-21 32 16.9	17500	30	9.5	fibr			
25206	1 01 20.3	-22 18 47.0	35765	45	7.7	fibr			
25208	1 01 28.1	-22 10 58.8	36588	36	8.3	fibr			
25209	1 01 32.4	-22 11 27.8	36907	49	5.6	fibr			
25212	1 01 33.3	-21 38 27.1	17594	57	5.0	fibr			
25214	1 01 39.5	-21 53 03.9	16228	82	3.5	e fibr			
25217	1 01 53.3	-22 20 51.3	18846	39	7.8	fibr			
25219	1 01 53.9	-22 02 28.8	16865	32	8.5	fibr			
25215	1 01 54.1	-22 30 08.4	18434	38	8.0	fibr			
25220	1 01 54.2	-21 40 15.5	17241	55	6.1	fibr			
25216	1 01 54.8	-22 29 20.9	18494	21	4	e fibr			
25221	1 01 57.4	-21 33 52.0	12394	81	4	e fibr			
25224	1 01 60.0	-21 48 30.3	16715	43	6.6	fibr			
25225	1 02 00.8	-21 48 33.0	17518	118	3	e fibr			
25227	1 02 02.9	-22 13 39.9	37480	57	4.7	e fibr			

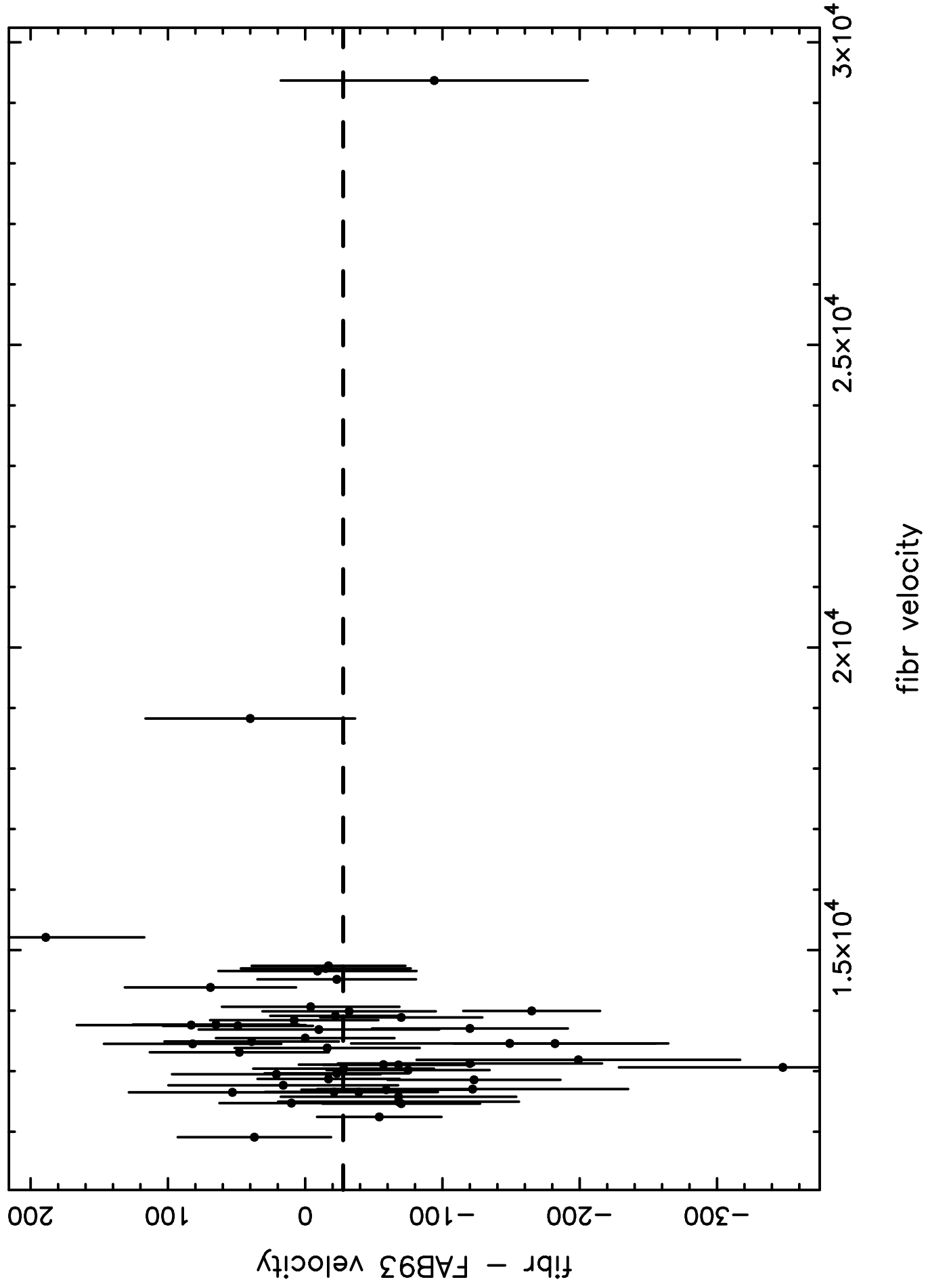
TABLE 2. (continued)

Ident.	α (1950)	δ (1950)	v_{\odot}	err	R	Ref	Id.Ref	\bar{v}_{\odot}	err
25228	1 02 05.9	-22 30 48.9	36933	44	6.1	fibr			
25223	1 02 06.1	-21 39 24.2	17623	75	2.8	fibr			
25222	1 02 13.2	-21 32 08.9	17473	55	6.1	fibr			
25238	1 02 16.8	-21 35 50.2	17548	56	5.5	fibr			
25235	1 02 17.5	-22 04 19.6	16732	39	7.4	fibr			
25229	1 02 19.2	-22 32 13.4	16285	33	8.3	fibr			
25239	1 02 24.1	-21 32 17.2	8010	18	5	e	fibr		
25240	1 02 25.4	-21 30 26.6	25827	65	4.0	e	fibr		
25230	1 02 27.4	-22 30 33.4	23611	80	4	e	fibr		
25245	1 02 32.7	-22 16 21.1	37378	56	4.5		fibr		
25243	1 02 39.8	-21 35 06.8	17486	44	6.4		fibr		
25244	1 02 42.1	-22 13 09.0	17034	51	6.6		fibr		
25247	1 02 44.2	-22 19 31.1	16845	31	9.5	e	fibr	16859	30
			16896	51	5.7	e	fibr		
25248	1 02 54.0	-21 41 02.8	15279	74	3.7	e	fibr		
25246	1 02 55.2	-22 33 03.3	36938	37	3	e	fibr		
25252	1 03 08.1	-21 44 51.8	12112	24	4	e	fibr	12095	30
			12047	40	7	e	fibr		
25253	1 03 08.5	-22 21 24.2	17206	28	11.4		fibr		
25254	1 03 18.3	-21 47 43.0	31166	42	5	e	fibr		
25256	1 03 20.1	-21 27 59.6	8456	38	7.5		fibr		

References for Table 2.

This paper: fibr = LCO fiber spectra; MK = Merrifield & Kent (1989); RC3 = de Vaucouleurs et al. (1991)





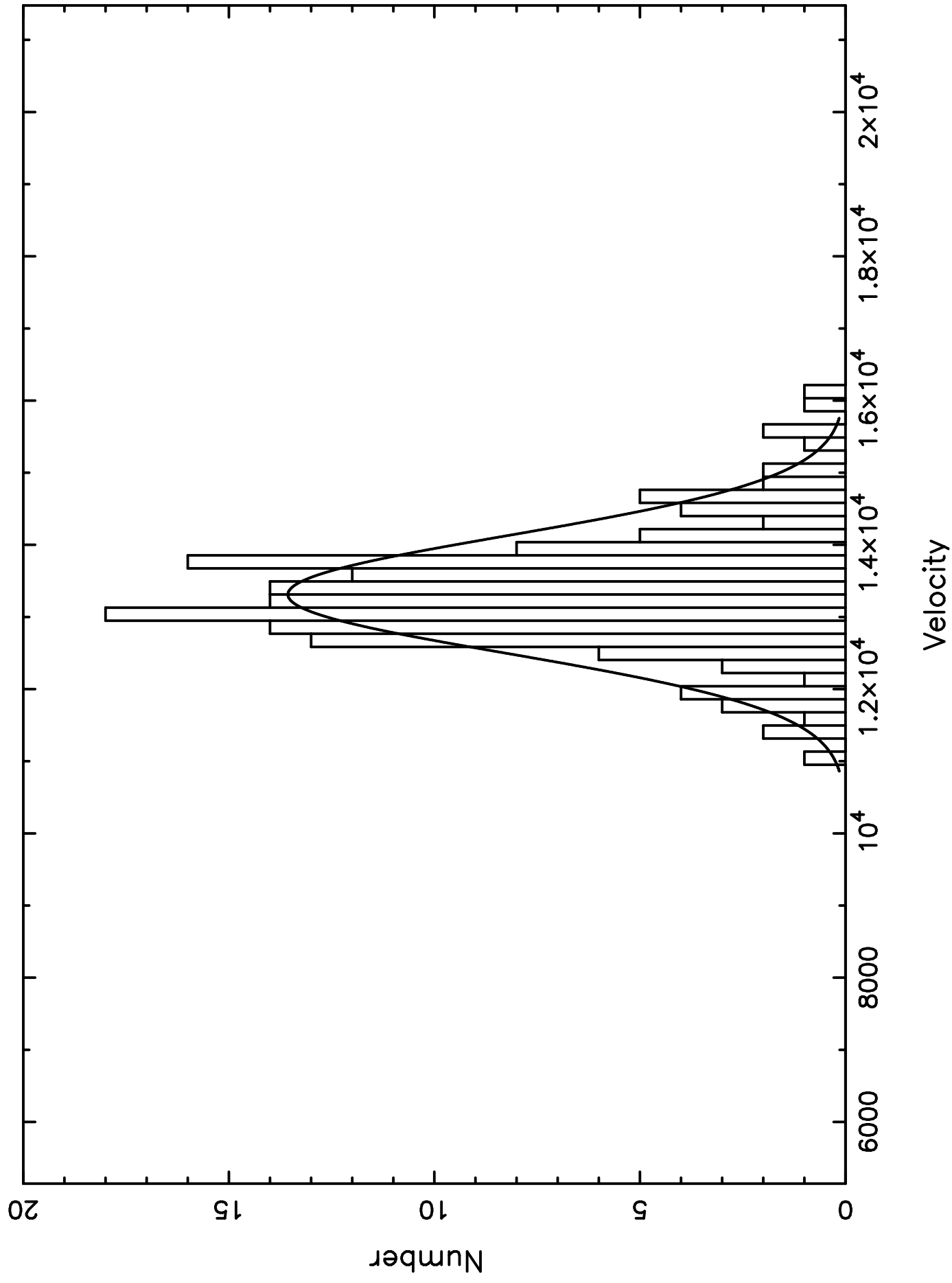
;

TABLE 3. 1D Statistics

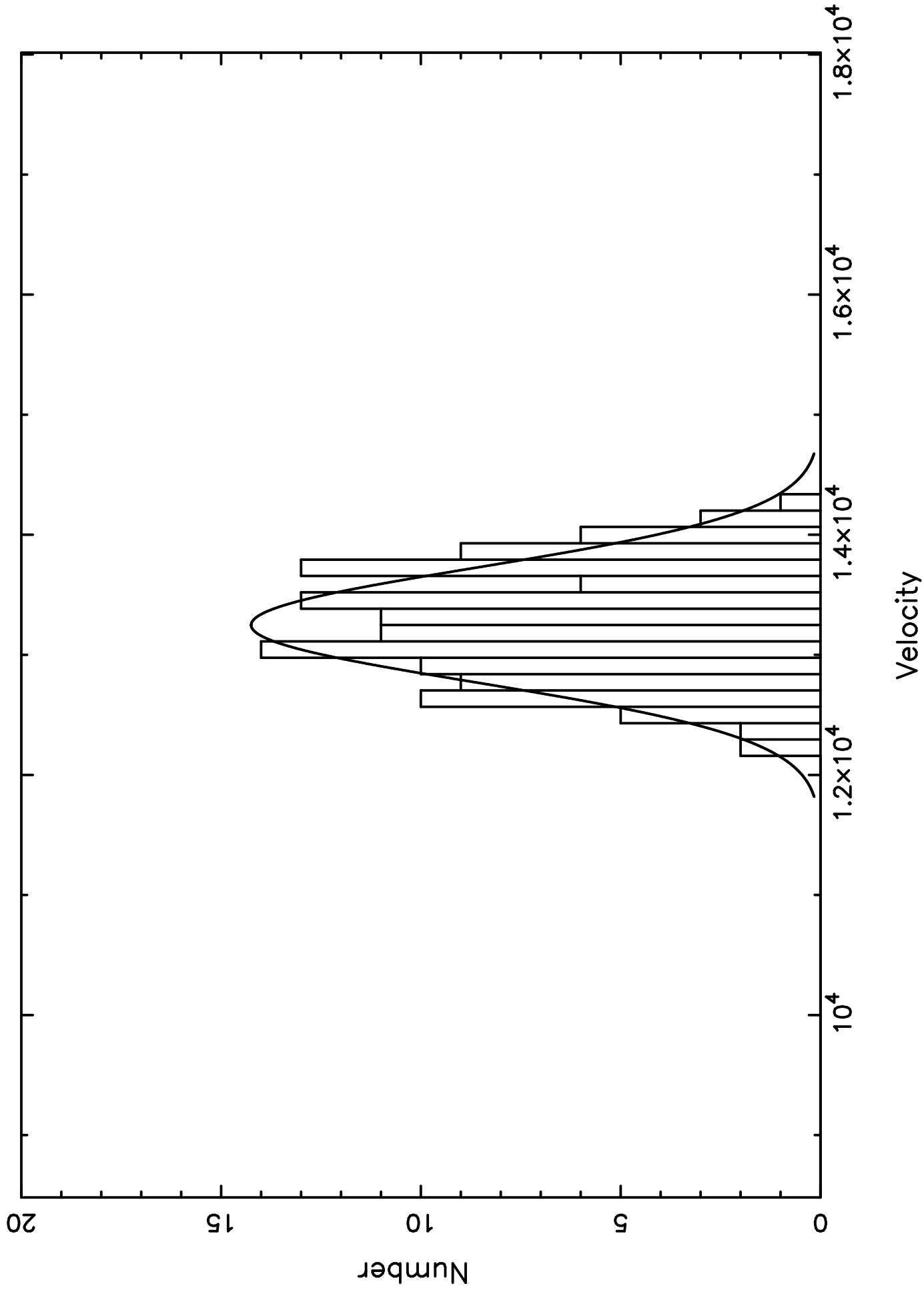
Cluster	N	C_{BI}^a	S_{BI}	skewness	kurtosis	asymmetry	tail ^b
A119	153	13228 (+103,-98)	778 (+122,-88)	0.407	3.962	0.545	1.183
A119 Group 1	11	11699 (+151,-183)	291 (+163,-83)	-0.712	2.797	-0.826	1.046
A119 Group 2	125	13248 (+71,-76)	472 (+41,-36)	-0.008	2.140	-0.180	0.855
A119 Group 3	17	14707 (+281,-104)	352 (+193,-152)	0.923	2.666	0.459	1.222
A133	120	16869 (+114,-114)	735 (+87,-72)	0.140	2.708	0.025	0.969

^aErrors on C_{BI} & S_{BI} are bootstrapped at 90% confidence intervals for 10000 bootstraps.^btail index has been normalized to a gaussian.

Abell 119



Abell 119 Group 2



;

TABLE 4. 2 and 3D Statistics

Cluster	N_{gal}	V_{pec}	Z_{score}^a	L_{RAT}	Δ	α	ϵ
A119	153	-5	0.007(+0.144,-0.142)	1.456	0.077	1.639	-4.718
A119 Group 1	11				-0.497	-1.058	1.232
A119 Group 2	125	34	0.072(+0.171,-0.180)	1.583	-1.787	0.474	0.651
A119 Group 3	17				-0.704	-0.757	0.934
A133	120	191	0.260(+0.166,-0.164)	2.415	4.523	1.128	0.956
A133($R < 1.5h^{-1}$ Mpc)	78	-	-	1.423	-	-	-

^aErrors are bootstrapped at 90% confidence intervals for 10000 bootstraps.

Abell 119

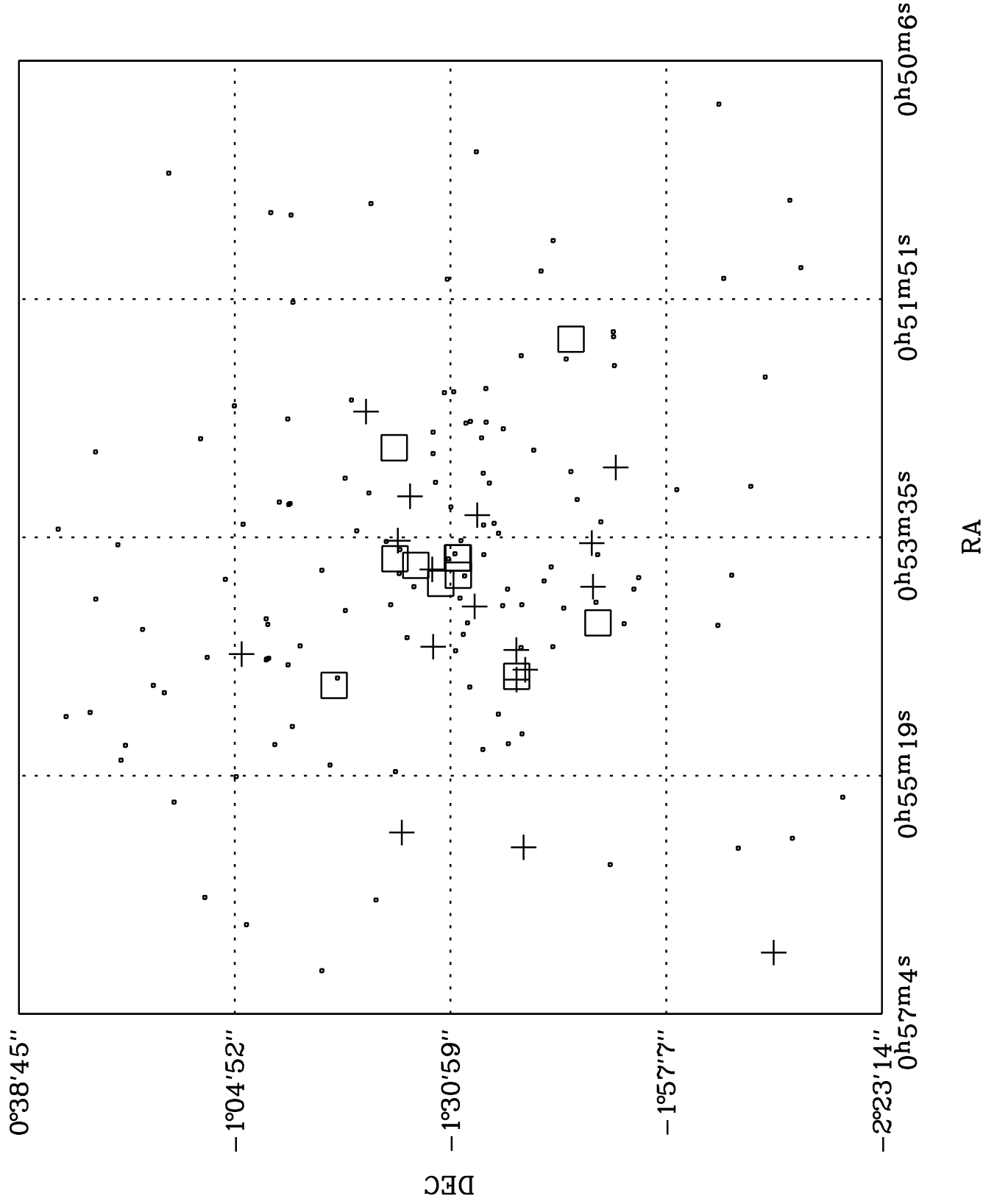


TABLE 5. Mass Estimators

Cluster	Group/Radius ^a	N_{gal}	$M_{virial}^{b,c}$	M_{pme}	M_{avg}	M_{med}	M_{vir}^{gray}
A119	Group 1 ^d	11	0.25 (0.06,1.55)	0.81 (0.35,1.32)	0.70 (0.23,1.22)	0.67 (0.18,0.98)	
A119	Group 2 R<0.5	30	1.62 (1.11,2.34)	1.78 (1.21,2.40)	1.28 (0.84,1.69)	1.21 (0.80,1.72)	1.00 ^e
A119	Group 2 R<1.5	98	3.05 (2.38,3.87)	3.78 (3.02,4.59)	2.97 (2.37,3.53)	2.91 (2.22,3.47)	
A119	Group 2 R<2.3	125	4.00 (3.23,4.94)	5.05 (4.15,6.02)	4.04 (3.33,4.72)	3.82 (3.06,4.57)	12.9 ^f
A119	Group 3 ^d	17	2.31 (1.02,5.08)	4.34 (1.54,7.80)	3.199 (0.97,5.25)	1.14 (0.30,2.93)	
A133	R<0.5	31	2.77 (1.71,4.37)	3.62 (2.01,5.49)	2.65 (1.46,3.89)	2.27 (1.20,3.43)	2.36 ^e
A133	R<1.5	78	7.79 (5.80,10.46)	10.97 (7.86,14.57)	8.220 (5.96,10.63)	7.09 (4.98,9.44)	7.30 ^e
A133	R<2.4	120	11.28 (8.86,14.36)	14.87 (11.41,18.72)	12.42 (9.71,15.13)	10.78 (8.03,13.67)	

^aMasses are $\times 10^{14}$ Solar Units. Errors are 90% bootstrapped confidence intervals.

^bRadii are h_{100}^{-1} Mpc

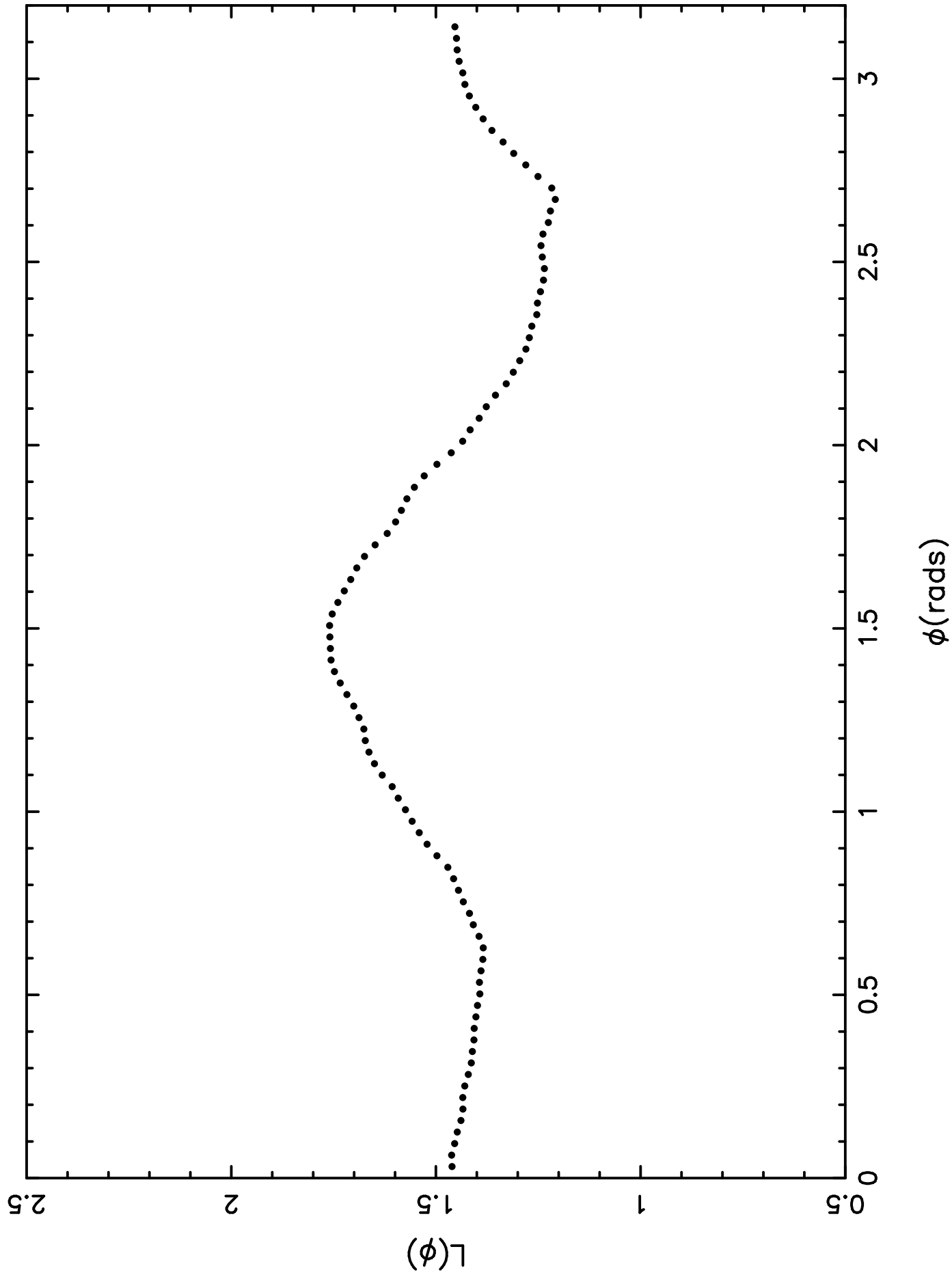
^cErrors are bootstrapped at 90% confidence intervals for 10000 bootstraps.

^dThese values *must* be taken in the context of infalling clumps, see the Mass section of Abell 119.

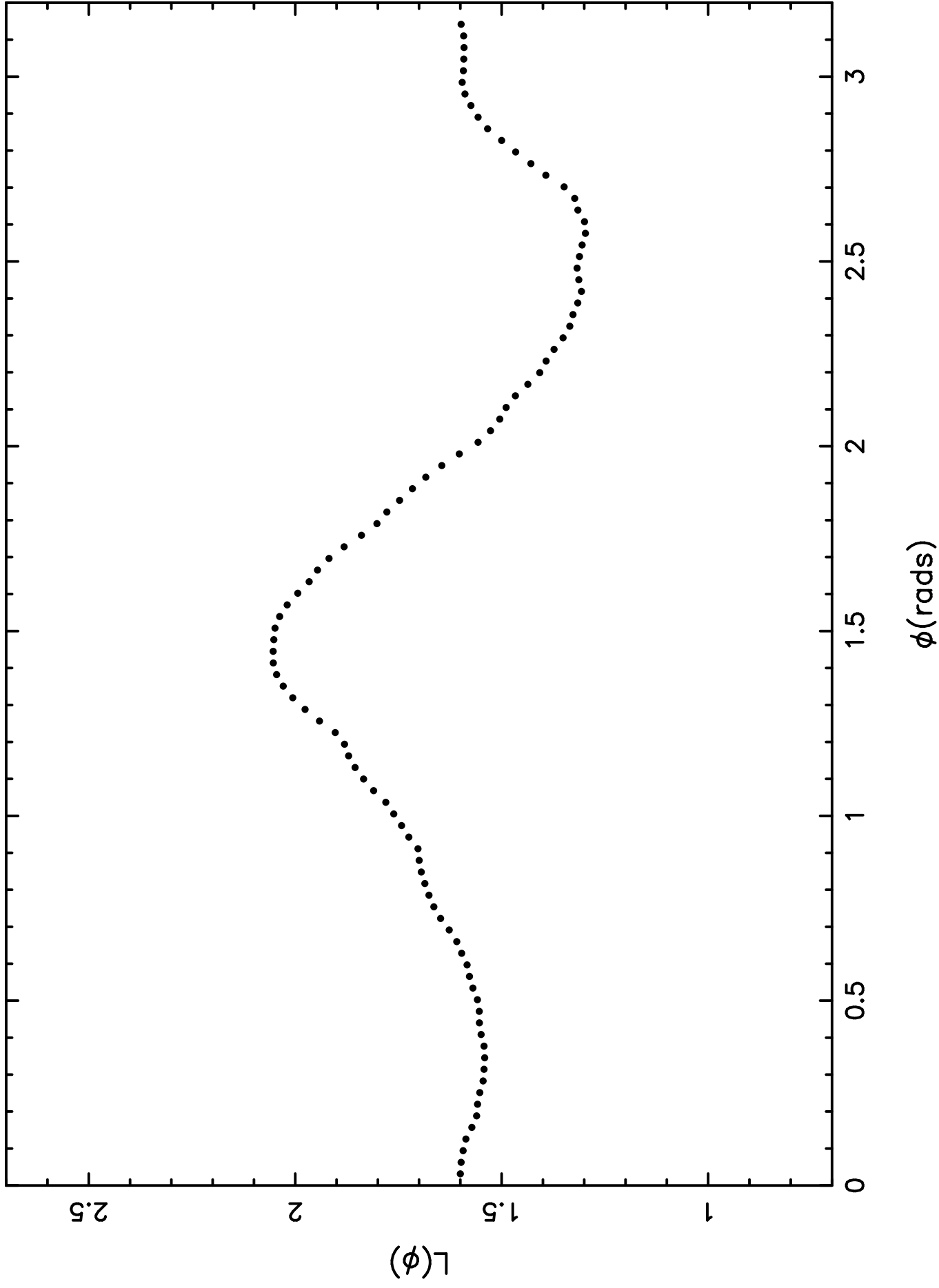
^eJones 1996

^fAbramopoulos & Ku 1983, Table 5, R<1.93 h^{-1} Mpc

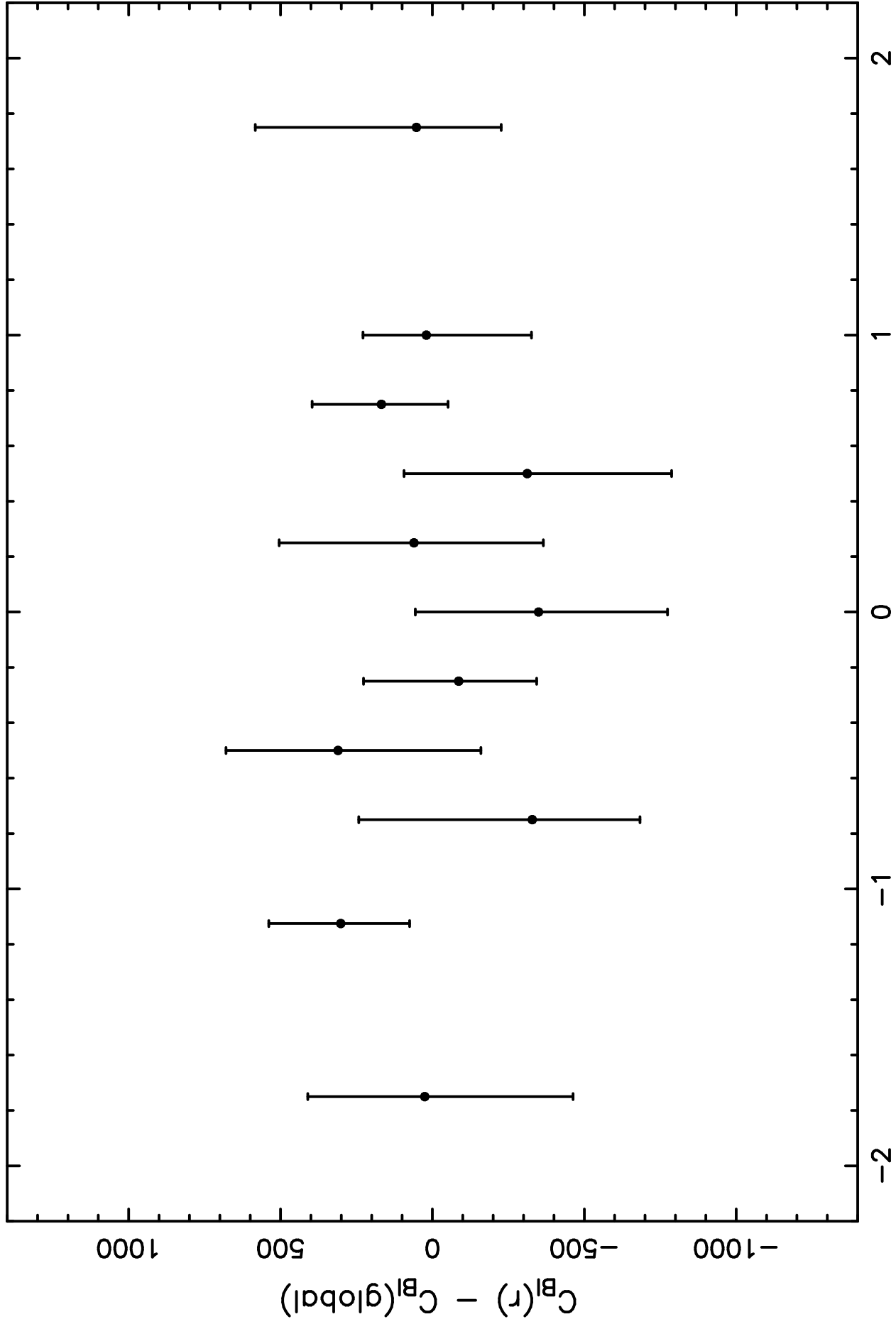
Abell 1119 Lee Statistic



Abell 119 Group 2 Lee Statistic

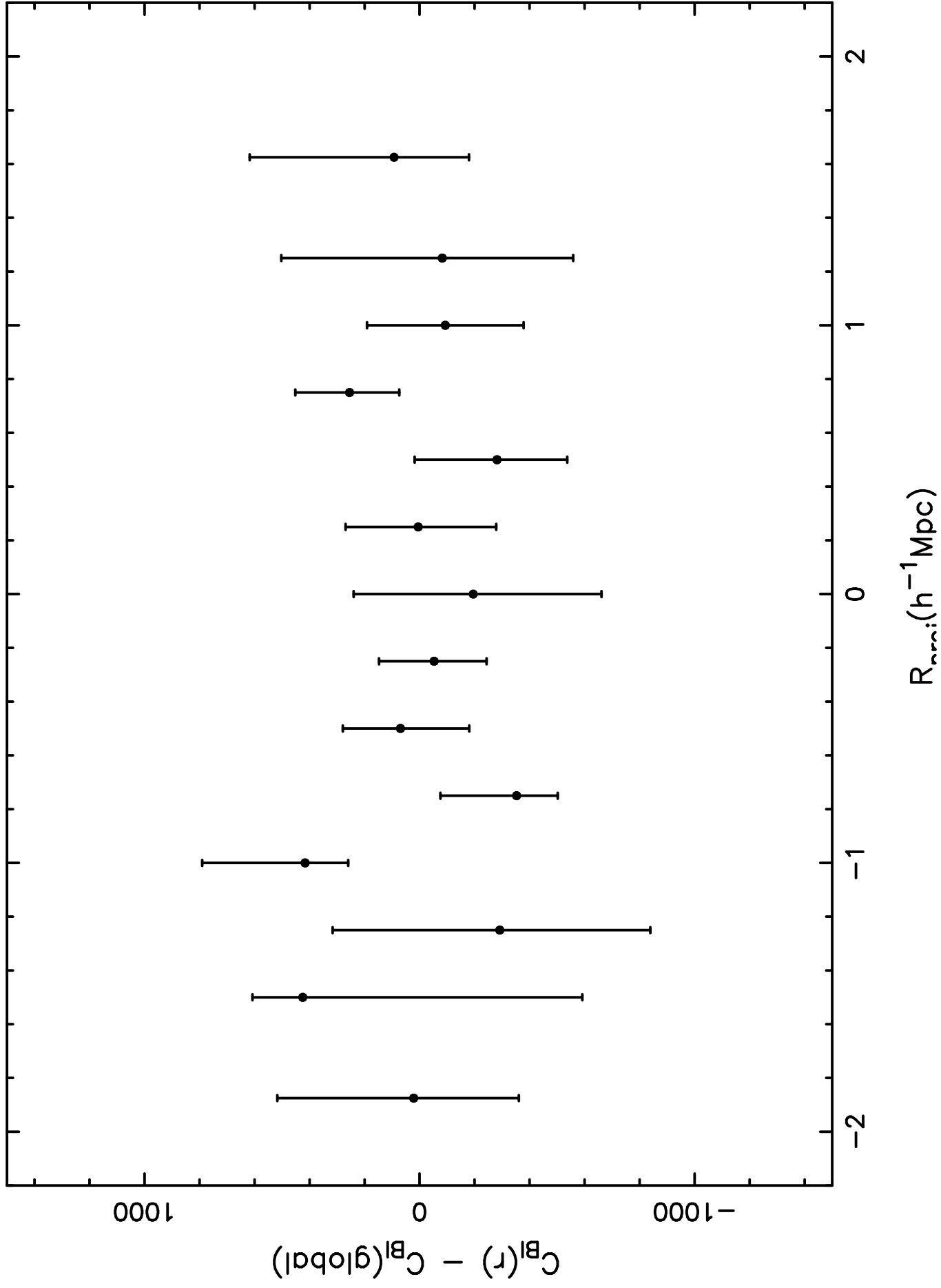


Abell 119

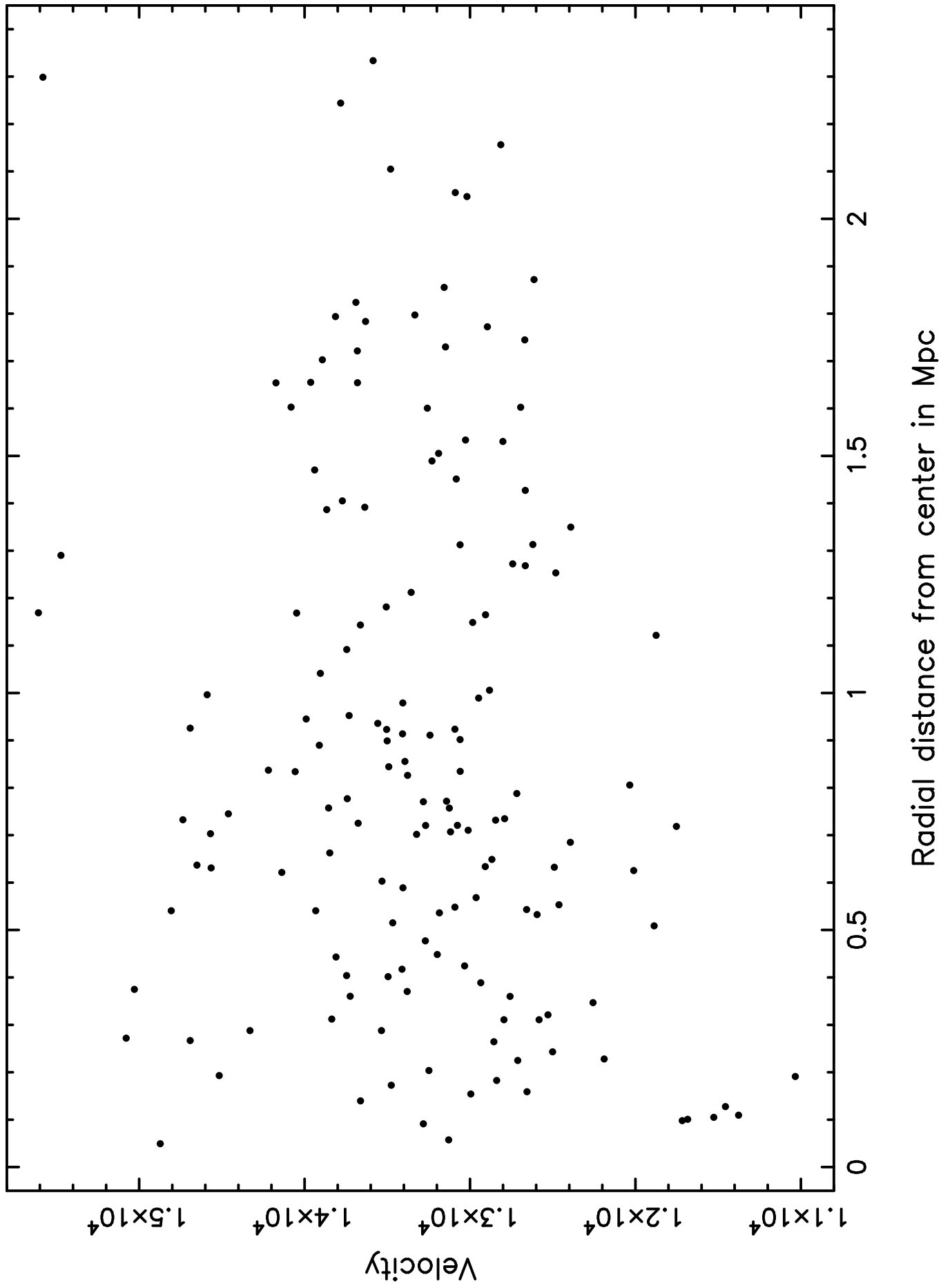


$R_{\text{bin}} (h^{-1} \text{Mpc})$

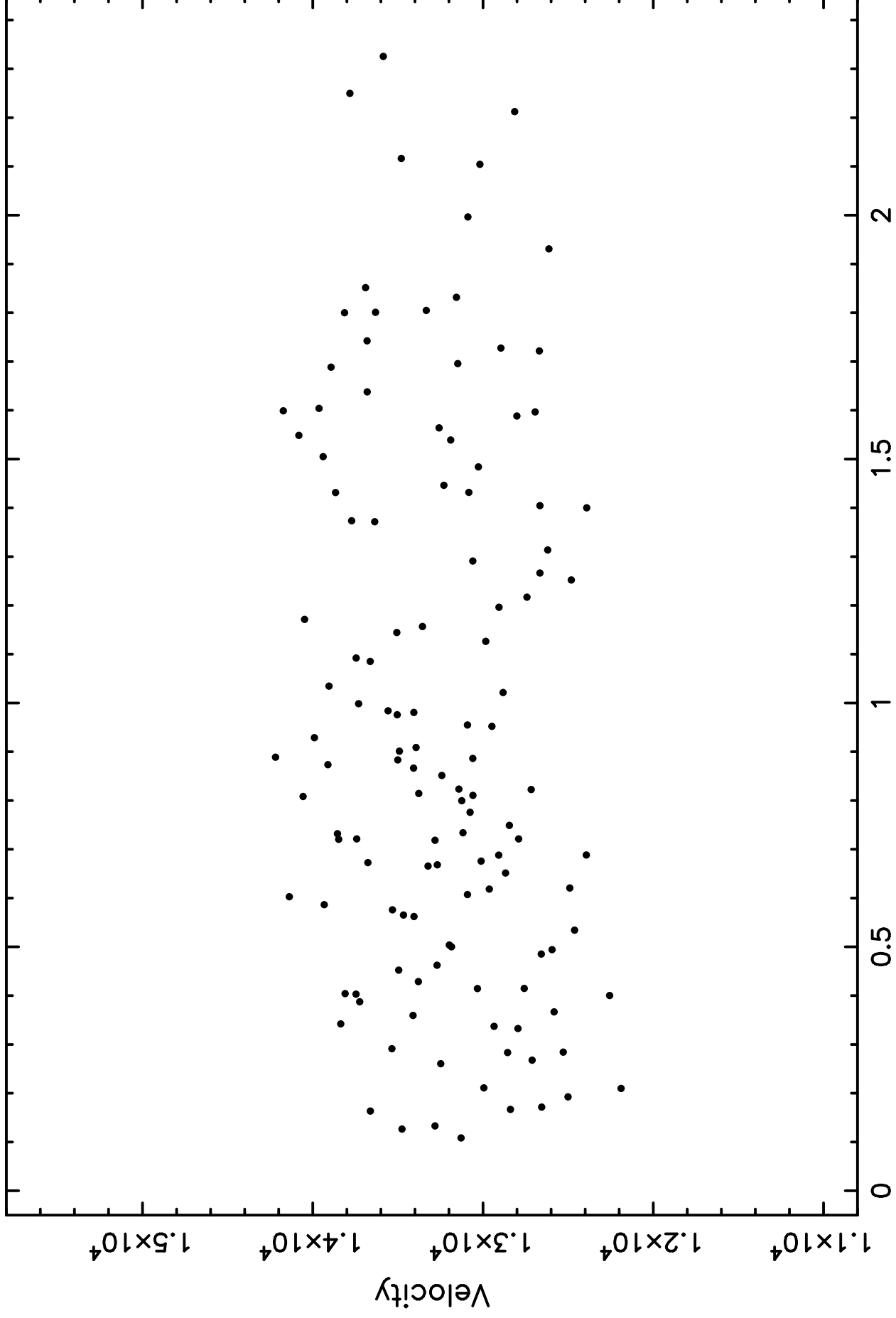
Abell 119 Group 2



Abell 119 Caustics

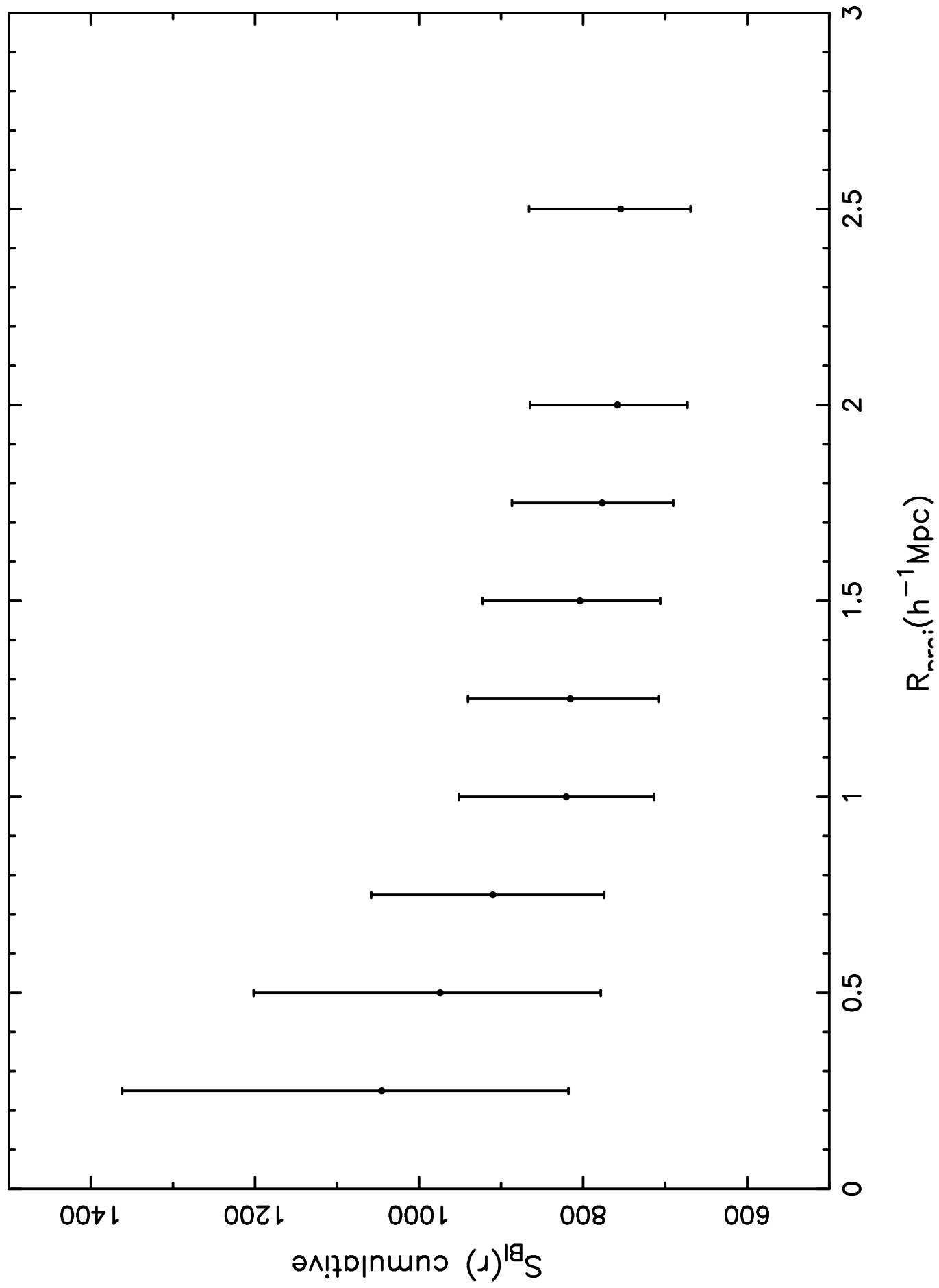


Abell 119 Group 2 Caustics

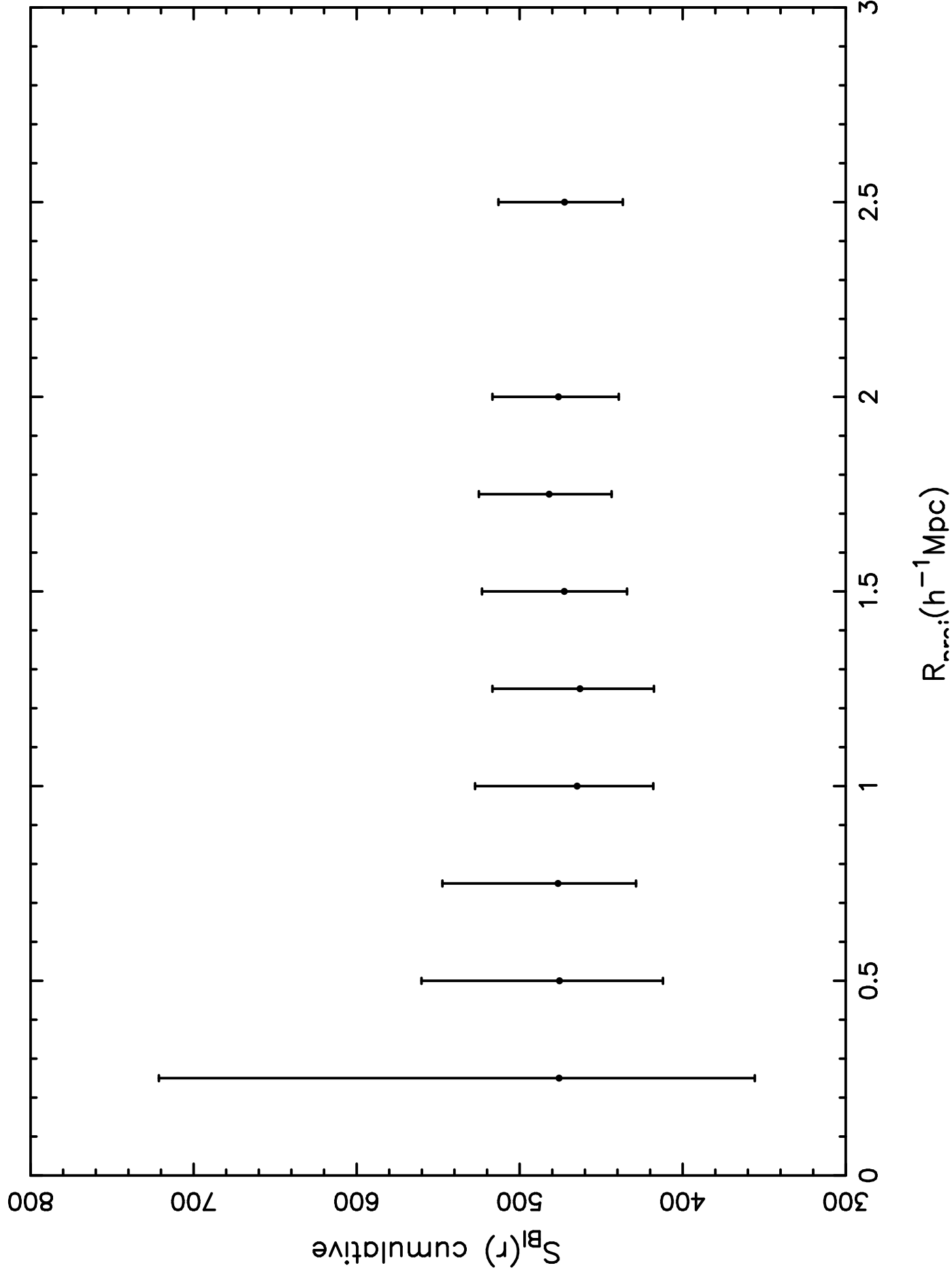


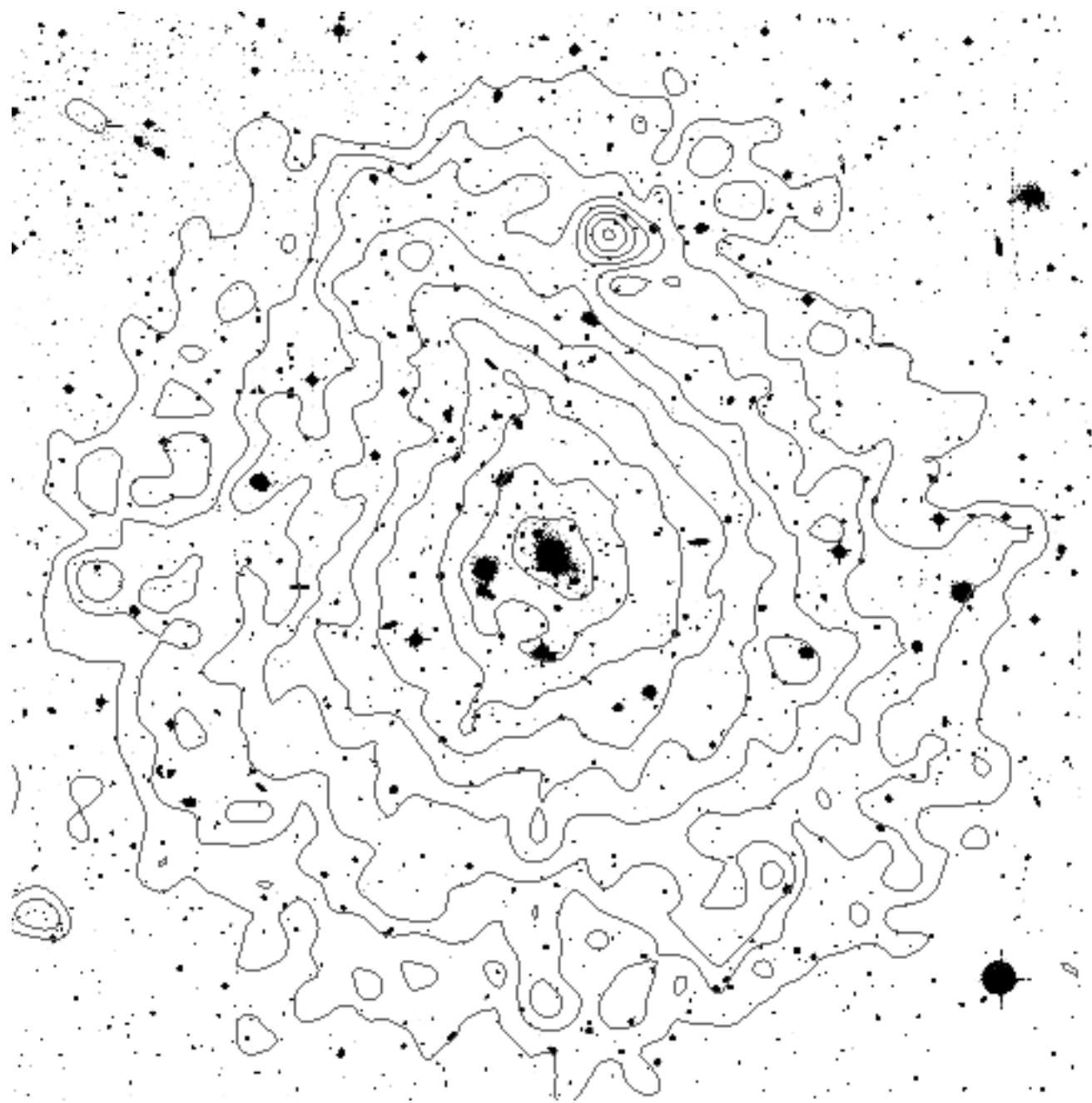
Radial distance from center in Mpc

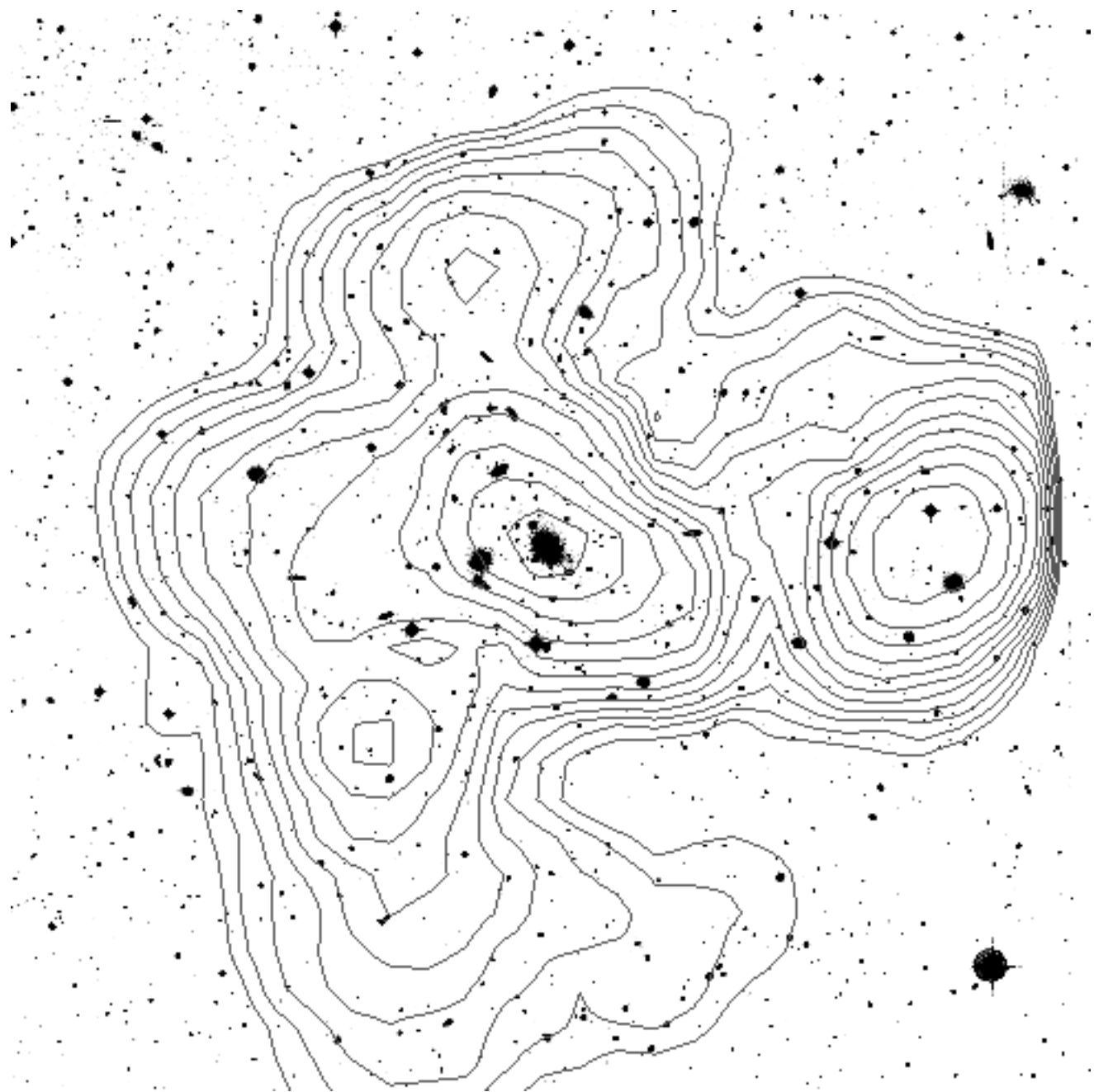
Abell 119



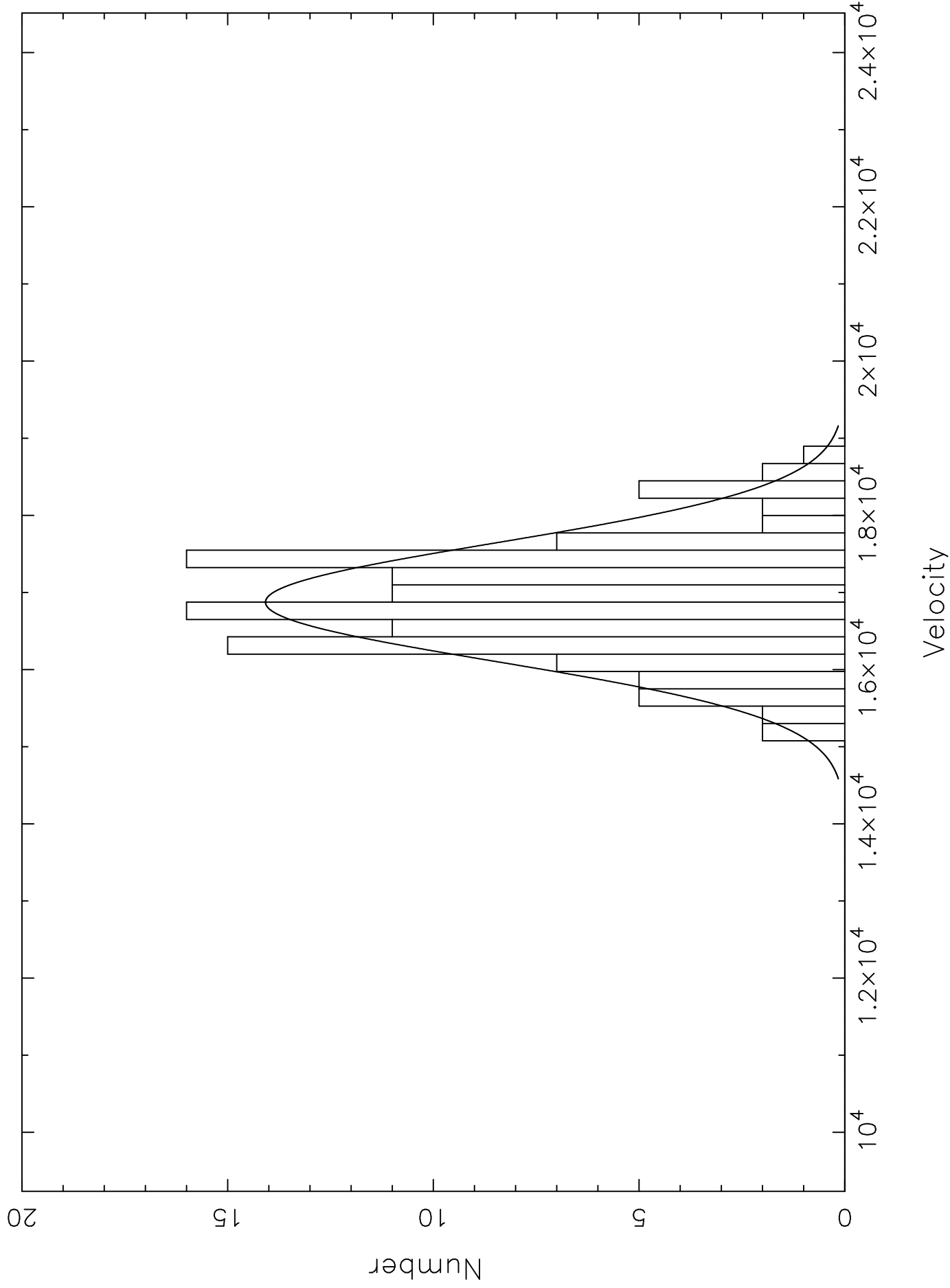
Abell 119 Group 2



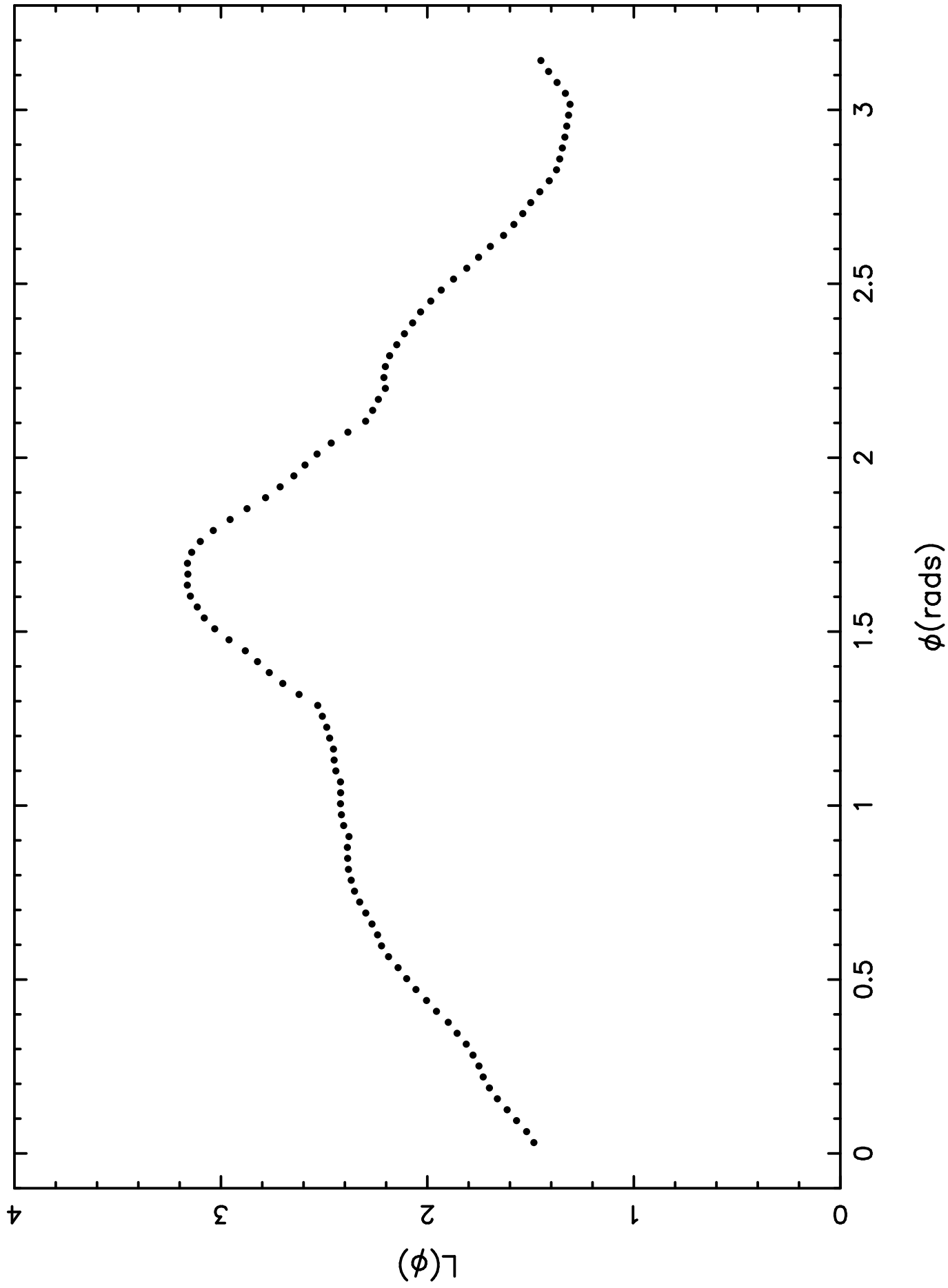




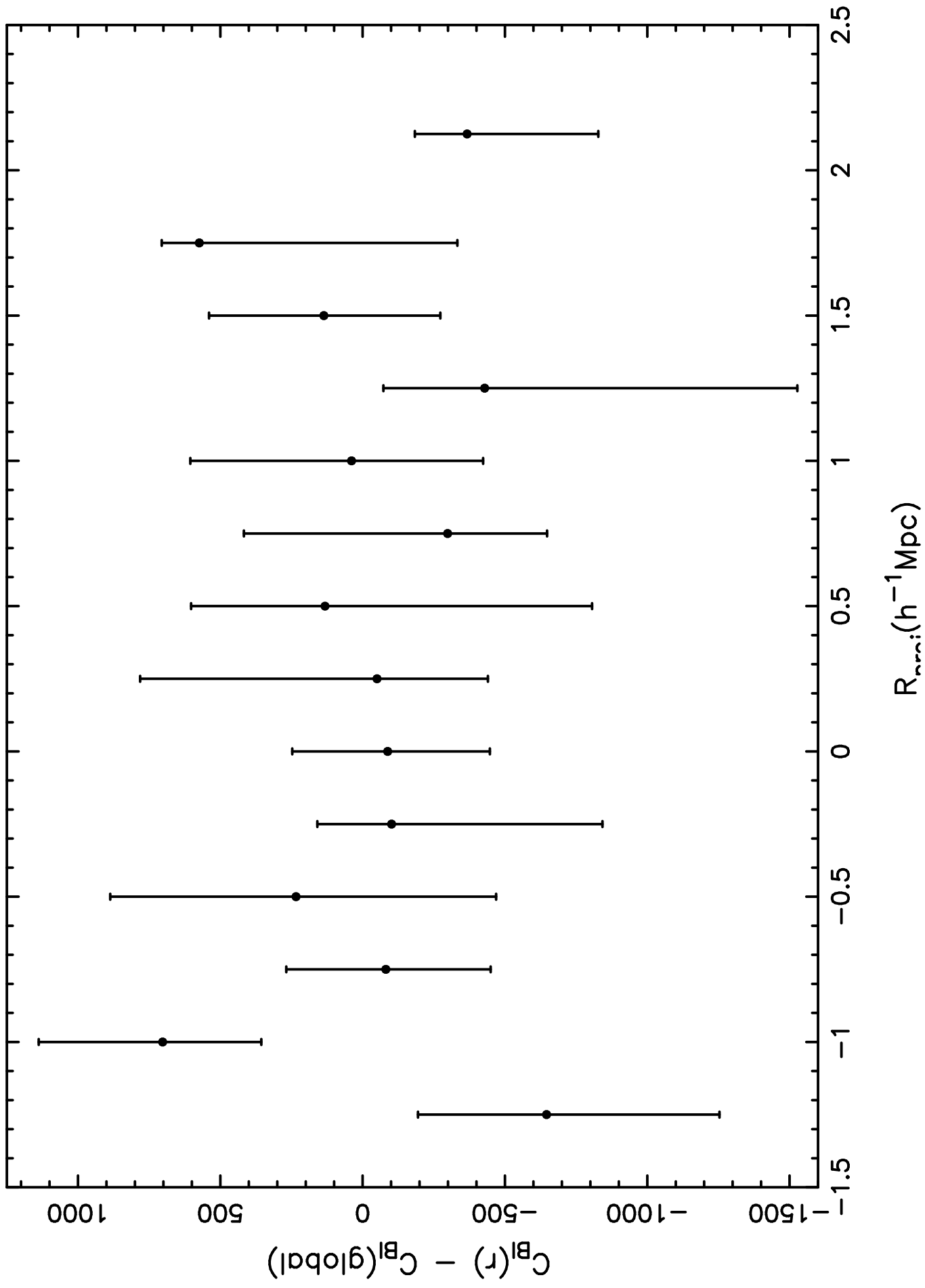
Abell 133



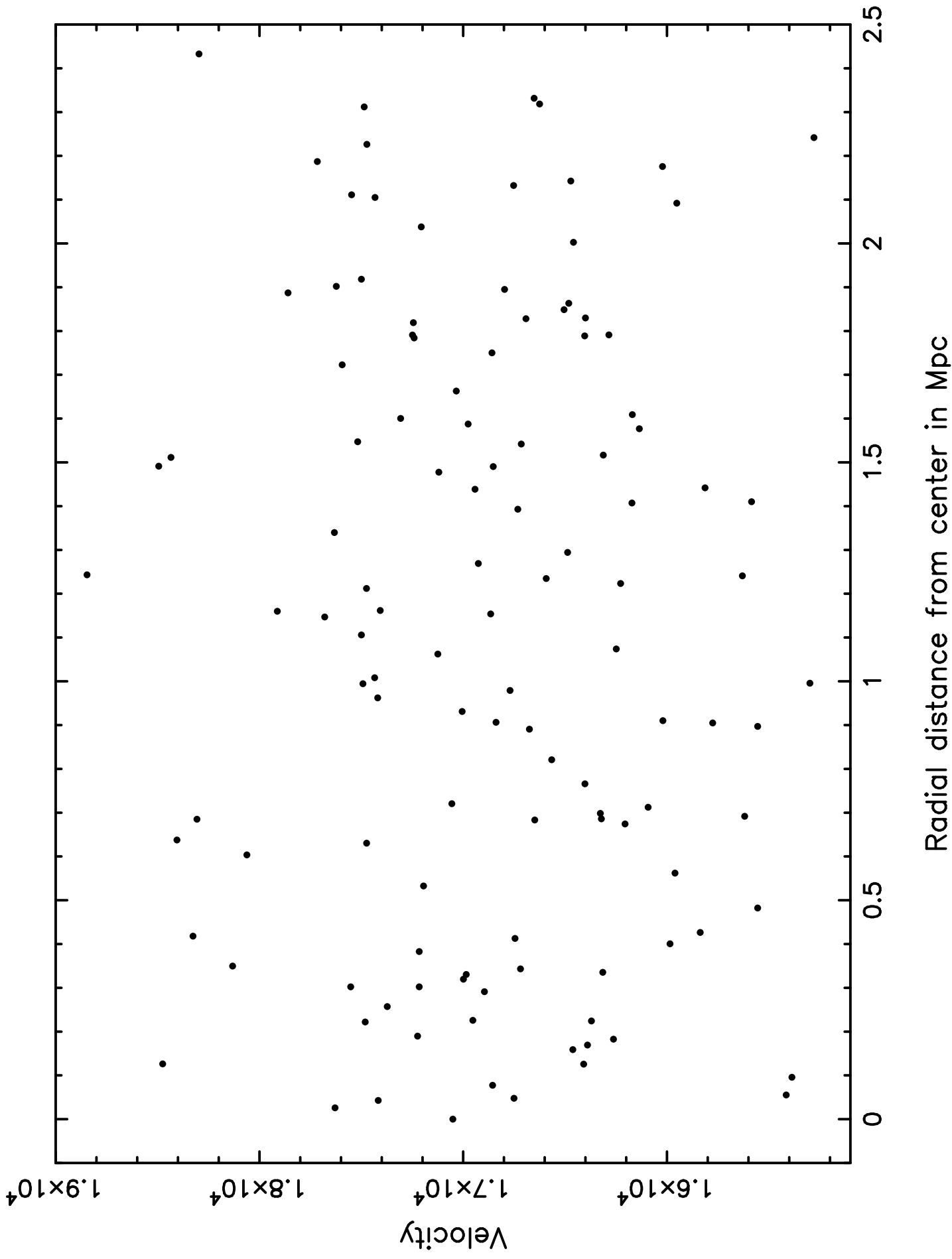
Lee statistic for Abell 133



Abell 133



Abell 133 Caustics



Abell 133

